Nonlinear Dyn (2020) 100:3529–3553
https://doi.org/10.1007/s11071-020-05707-2

ORIGINAL PAPER

A new adaptive neural control scheme for hypersonic vehicle with actuators multiple constraints

Changxin Luo · Humin Lei · Jiong Li · Chijun Zhou

Received: 11 December 2019 / Accepted: 17 May 2020 / Published online: 8 June 2020

Abstract A new adaptive neural control method, with the actuators multiple constraints of amplitude and rate into consideration, is proposed in this paper for the flexible air-breathing hypersonic vehicle (AHV). In order to better reflect the characteristics of the actual AHV model, we regard the AHV as a completely unknown non-affine system in the control law design process, which is different from the existing AHV control methods, thus ensuring the reliability of the designed control law. On the basis of the implicit function theorem, the radial basis function neural network (RBFNN) is introduced to approximate the model. Meanwhile, the minimum learning parameter algorithm is adopted to adaptively adjust the weight vector of RBFNN, then the design of the ideal control law is completed. When the amplitude and rate of the actuator are saturated, the designed novel auxiliary error compensation system is used to effectively compensate for the ideal control law, and the stability of the closed-loop control system is proved via the Lyapunov stability theory. In addition, to avoid the "explosion of terms" problem in the control law design process, the finite-time-convergence-differentiator is introduced to accurately estimate the differential signal. Finally, the effectiveness of the control method designed in this paper is verified by simulation.

Keywords Air-breathing hypersonic vehicle · Auxiliary error compensation system · Adaptive neural control · Implicit function theorem · Minimum learning parameter algorithm

C. Luo (✉)
Graduate School, Air Force Engineering University, Xi'an 710051, China
e-mail: 1710794652@qq.com

H. Lei · J. Li · C. Zhou
Air and Missile Defense College, Air Force Engineering University, Xi'an 710051, China

List of symbols

m	Vehicle mass
g	Gravitational constant
I_{yy}	Moment of inertia
ζ_i	Damping ratio for flexible modes η_i
ω_i	Natural frequency for flexible modes η_i
$\tilde{\psi}_i$	Constrained beam coupling constant for η_i
L_{f}	The length of forward beam
L_{a}	The length of aft beam
$\hat{m}_{\mathrm{f}}$	Mass distribution of forward beam
$\hat{m}_{\mathrm{a}}$	Mass distribution of aft beam
$\phi_{\mathrm{f}}(\cdot)$	Structural mode shape of forward beam
$\phi_{\mathrm{a}}(\cdot)$	Structural mode shape of aft beam
$\bar{q}$	Dynamic pressure
S	Reference area
z_{T}	Thrust moment arm
$\bar{c}$	Aerodynamic chord
$\bar{\rho}$	Air density at height h
h_0	Nominal altitude
$\bar{\rho}_0$	Air density at the altitude h_0

$1/h_s$	Air density decay rate
c_{e}	Elevator coefficient
$C_T^{\alpha^i}$	ith order coefficient of α in T
$C_D^{\alpha^i}$	ith order coefficient of α in D
$C_T^{\delta e^i}$	ith order coefficient of δ_{e} in T
$C_D^{\delta e^i}$	ith order coefficient of δ_{e} in D
C_T^0	Constant coefficient in T
C_D^0	Constant coefficient in D
C_L^0	Constant coefficient in L
C_L^{α}	Coefficient of α in L
$C_L^{\delta e}$	Coefficient of δ_{e} in L
$C_{M,\alpha}^{\alpha^i}$	ith order coefficient of α in M
$C_{M,\alpha}^0$	Constant coefficient in M
$N_j^{\alpha^i}$	ith order contribution of α to N_j
N_i^0	Constant term in N_i
$N_2^{\delta e}$	Contribution of δ_{e} to N_2
$\beta_i(h, \bar{q})$	ith trust fit parameter

1 Introduction

The air-breathing hypersonic vehicle is a new type of aircraft flying in the near space at a speed of more than 5 Ma. It has the advantages of fast flight speed, strong penetration ability and high effect cost ratio, making it the prior development direction of the world's aerospace powers for the air right [1–3]. However, the air density, pressure, radiation, temperature, and wind field in the AHV's flight airspace are greatly different from those in the environment where the traditional aircraft is located. This results in AHV's exhibiting more significant cross-coupling, nonlinearity, nonminimum phase behavior, and model uncertainty than traditional aircraft in terms of dynamics [4, 5].

These characteristics of AHV bring great challenges to the design of control system, making AHV's flight control a frontier issue in the control field. Considering that Scramjet is extremely sensitive to flight attitude and to save fuel, AHV should avoid lateral maneuvers in actual flight as far as possible [6]. Therefore, the modeling and control research of AHV is mainly carried out in its longitudinal motion plane. In order to solve this kind of complex control problems, many scholars have carried out research in recent years and achieved many results.

Some have carried out research on control methods based on the idea of linear parameter-varying (LPV) [7–15]. For rigid body model of AHV, Gang Gao and Jinzhi Wang firstly obtain the LPV model using the feedback linearization technique and then design a robust controller via H_∞ method, which achieves desired tracking performance with well robustness [7]. However, because they fail to consider the flexible modes of the AHV, the designed control method is not applicable to the flexible AHV model. In Ref. [8], for flexible hypersonic vehicles, the reference tracking problem is investigated via a novel switched LPV framework. Hu Chaofang et al. propose a novel passive fault-tolerant control method based on polytopic LPV for AHV [9]. In terms of basic theory, Ref. [10] studies the design of H_-/H_∞ fault detection observer for LPV descriptor systems, and Ref. [11] studies the problem of asymptotic stability for switched linear systems. Aiming at the control problem of hypersonic vehicle, LPV anti-windup model reference controller and finite-time LPV sliding mode controller are designed in [12, 13], respectively. Although the LPV-based control method has achieved certain effects, it will offset some beneficial nonlinear characteristics of AHV, resulting in wasting the effectiveness of AHV actuators.

Many people choose to directly design the controller for the nonlinear model of AHV, and backstepping control is such an important method. Using flexible AHV model as a controlled object and converting it to strict feedback form, Refs. [16, 17] provide two effective backstepping control methods, respectively. Combining backstepping scheme and barrier Lyapunov functions, Refs. [18, 19] study the finite-time tracking control problem of hypersonic vehicle. For discrete-time switched piecewise-affine systems, Yan-zheng Zhu and Wei Xing Zheng investigate the asymptotic stability analysis and state-feedback control [20]. Based on extended state observer and disturbance observer, anti-disturbance backstepping control and robust backstepping control are designed in Refs. [21, 22], respectively. In order to deal with uncertainties and external disturbances in the tracking process, Ref. [23] proposes a robust backstepping method based on a novel tracking differentiator, and a fixed-time disturbance observer-based fixed-time backstepping method is designed in Ref. [24]. These methods have achieved good results, but most of them are based on backstepping control

methods, which require the continuous design steps of virtual control laws, resulting in a cumbersome design process.

Many scholars combine artificial intelligence with automatic control, and propose some intelligent control methods. Among them, adaptive neural control [25–27] and fuzzy control [28] occupy an important position. By treating AHV as an unknown affine system, Bu and Wu [29] propose an adaptive neural control strategy, in which a neural network is employed for the unknown function approximation. Also based on neural networks, Refs. [30, 31] propose integral sliding mode control method and stochastic adaptive attitude control method to solve the control problem of hypersonic vehicle, respectively. In order to improve the transient performance of the control system, Zhao and Liang [32] propose a prescribed performance dynamic neural network control method. Aiming at robust stability of system, the data-driven realization of the closed-loop stability margin has been studied in Ref. [33]. Based on fuzzy logic system, Refs. [34, 35] design robust tracking controller and fuzzy tracking controller, respectively. To improve the performance of attitude command tracking, Liu et al. [36] propose a fuzzy fast terminal sliding mode control method. These methods have been proved to have good control effects, but most of them simplify the motion model of the AHV to the affine form of the control input, which has certain limitations.

It is worth noting that the height and attitude of AHV's longitudinal motion are mainly controlled by elevators, the efficiency of the elevator will decrease significantly as the flying height increases [6]. On the other hand, the AHV can be affected by unknown airflows such as turbulence and gust during the flight process. So the phenomenon of elevator saturation is easy to appear when AHV flying at high altitude. Once the actuators reach saturation, it may cause failure of the control system [37]. Some scholars have conducted research on anti-saturation control method of AHV. By designing an adaptive law to approximate the actuator constraints dynamics, Xu et al. [38] design a neural controller via time-scale decomposition, which guarantees the uniformly ultimately boundedness of the system. But they only consider the throttle setting constraint of the engine. An adaptive terminal sliding mode control method based on the inner-loop and outer-loop systems is designed via using multilayer neural networks for the approximation of the saturation property of two control inputs in Ref. [37]. Similar to Refs. [37, 38], through proposing adaptive laws to estimate the information of input saturation constraint online, Bing et al. [39] design an adaptive fault tolerant control strategy, which makes AHV track the desired trajectories in the presence of actuator fault and input saturation. In Ref. [40], in order to deal with actuator magnitude constraints, two auxiliary systems are constructed to generate certain compensating signals. Guangfu and Chen [41] introduce a sigmoid function to approximate the saturation and guarantee that the control input is bounded. In Ref. [42], Zhonghua Wu et al. overcome the problem of actuator constraint with the utilization of an assistant compensation system. Although Refs. [37–42] solve the problem of AHV control input constraints to some extent, none of them theoretically proves that the tracking error is bounded when the actuator is saturated. In view of this, Xiangwei and Xiaoyan [43] construct an auxiliary system to compensate the desired control laws thus ensuring the stability of the closed-loop control system and the boundedness of the tracking error. However, most of the existing AHV anti-saturation control methods only consider the case where the amplitude of the actuator is constrained, and do not consider the problem of its rate constraint.

In general, the above studies on AHV control methods have achieved good results, but there are still some shortcomings. Firstly, forcing AHV's non-affine motion model into an affine model will inevitably result in the loss of certain key dynamic characteristics. The control law designed based on the simplified affine model will have the risk of partial or complete failure. Secondly, the use of backstepping design strategy requires repeated derivation of the virtual control law, which leads to a cumbersome control law design process and will have a certain adverse effect on the final control accuracy. Thirdly, the above studies on AHV anti-saturation control only consider the condition of actuator amplitude constraint without any compensation for its rate constraint, which will cause the closed-loop control system to destabilize when the control input rate is saturated.

In view of the above shortcomings, there are three contributions in this paper. The first is to design the control law with AHV as a completely unknown non-affine system to enhance the reliability of the controller. In combination with the implicit function theorem, RBFNN is used to approximate the model by

designing the appropriate adaptive law, then to complete the design of the non-affine control law. The second is to design a new type of adaptive neural controller by equivalently transforming the AHV model, which avoids the cumbersome backstepping design process and ensures the control accuracy. The third is to further consider the more realistic situation in which both the amplitude and rate of the actuator are constrained. A novel auxiliary error compensation strategy is designed to effectively compensate for the ideal control law, thus guaranteeing the stability of the closed-loop control system and the boundedness of the tracking error when the amplitude and rate of the actuator are simultaneously constrained. The simulation results verify the effectiveness and superiority of the proposed method.

The rest of this paper is structured as follows: Sect. 2 describes the longitudinal motion model of AHV and prepares for the design of controller. And the proposed adaptive neural control method is presented in Sect. 3. Then, Sect. 4 analyzes the stability of the proposed control method. Moreover, the simulation results are shown in Sect. 5 to illustrate the effectiveness of designed controller. Finally, Sect. 6 summarizes the work of this paper and gives an outlook for the future work.

2 AHV model and preliminaries

This section introduces the longitudinal motion model of AHV and prepares for the design of subsequent control laws. Firstly, in Sect. 2.1, the control-oriented AHV longitudinal motion parameter fitting model is described in detail. Then, the control objective of this paper is explained in Sect. 2.2 and the AHV model is converted equivalently to facilitate the design of the controller later. Thirdly, in order to better design the subsequent adaptive law, RBFNN is briefly introduced in Sect. 2.3.

2.1 Model description

Based on the study of Bolender and Doman [44], Parker, a scholar of the US Air Force Research Laboratory, establishes a control-oriented AHV longitudinal motion parameter fitting model by neglecting some weak coupling and slow dynamics in the model [45].

$$\dot{V} = \frac{T\cos(\theta-\gamma) - D}{m} - g\sin\gamma \tag{1}$$

$$\dot{h} = V\sin\gamma \tag{2}$$

$$\dot{\gamma} = \frac{L + T\sin(\theta-\gamma)}{mV} - \frac{g}{V}\cos\gamma \tag{3}$$

$$\dot{\theta} = Q \tag{4}$$

$$\dot{Q} = \frac{M + \tilde{\psi}_1\ddot{\eta}_1 + \tilde{\psi}_2\ddot{\eta}_2}{I_{yy}} \tag{5}$$

$$k_1\ddot{\eta}_1 = -2\zeta_1\omega_1\dot{\eta}_1 - \omega_1^2\eta_1 + N_1 - \tilde{\psi}_1\frac{M}{I_{yy}} - \frac{\tilde{\psi}_1\tilde{\psi}_2\ddot{\eta}_2}{I_{yy}} \tag{6}$$

$$k_2\ddot{\eta}_2 = -2\zeta_2\omega_2\dot{\eta}_2 - \omega_2^2\eta_2 + N_2 - \tilde{\psi}_2\frac{M}{I_{yy}} - \frac{\tilde{\psi}_2\tilde{\psi}_1\ddot{\eta}_1}{I_{yy}} \tag{7}$$

with

$$\begin{cases} k_1 = 1 + \dfrac{\tilde{\psi}_1}{I_{yy}} \\ k_2 = 1 + \dfrac{\tilde{\psi}_2}{I_{yy}} \\ \tilde{\psi}_1 = \displaystyle\int_{-L_f}^{0} \hat{m}_f\xi\phi_f(\xi)\mathrm{d}\xi \\ \tilde{\psi}_2 = \displaystyle\int_{0}^{L_a} \hat{m}_a\xi\phi_a(\xi)\mathrm{d}\xi \end{cases} \tag{8}$$

where velocity V, altitude h, flight-path γ, pitch angle θ and pitch rate Q are the five rigid-body states; the four flexible modes η_1, $\dot{\eta}_1$, η_2, $\dot{\eta}_2$ denote the first two bending modes of the fuselage. Force map of a AHV model is shown in Fig. 1. The approximations of thrust T, drag D, lift L, pitching moment M and the generalized forces $N_i(i=1,2)$ are expressed as Eq. (9).

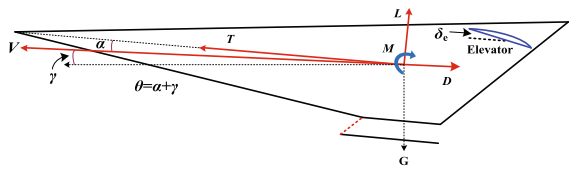

Fig. 1 Force map of a AHV model

$$\begin{cases} T \approx C_T^{\alpha^3}\alpha^3 + C_T^{\alpha^2}\alpha^2 + C_T^{\alpha}\alpha + C_T^0 \\ D \approx \bar{q}S\left(C_D^{\alpha^2}\alpha^2 + C_D^{\alpha}\alpha + C_D^{\delta_e^2}\delta_e^2 + C_D^{\delta_e}\delta_e + C_D^0\right) \\ L \approx \bar{q}S\left(C_L^{\alpha}\alpha + C_L^{\delta_e}\delta_e + C_L^0\right) \\ M \approx z_T T + \bar{q}S\bar{c}\left[C_{M,\alpha}^{\alpha^2}\alpha^2 + C_{M,\alpha}^{\alpha}\alpha + C_{M,\alpha}^0 + c_e\delta_e\right] \\ N_1 \approx N_1^{\alpha^2}\alpha^2 + N_1^{\alpha}\alpha + N_1^0 \\ N_2 \approx N_2^{\alpha^2}\alpha^2 + N_2^{\alpha}\alpha + N_2^{\delta_e}\delta_e + N_2^0 \\ C_T^{\alpha^3} = \beta_1(h,\bar{q})\Phi + \beta_2(h,\bar{q}) \\ C_T^{\alpha^2} = \beta_3(h,\bar{q})\Phi + \beta_4(h,\bar{q}) \\ C_T^{\alpha} = \beta_5(h,\bar{q})\Phi + \beta_6(h,\bar{q}) \\ C_T^0 = \beta_7(h,\bar{q})\Phi + \beta_8(h,\bar{q}) \\ \bar{q} = \frac{1}{2}\bar{\rho}V^2 \\ \bar{\rho} = \bar{\rho}_0 \exp\left(\frac{h_0 - h}{h_s}\right) \end{cases} \tag{9}$$

where $\alpha = \theta - \gamma$ is angle of attack; fuel equivalence ratio Φ and elevator angular deflection δ_e are control inputs. The definitions of the relevant parameters in the above model are shown in Nomenclature. The specific values can be found in Ref. [45].

2.2 Control objective and model conversion

According to Ref. [29], and by combining Eqs. (1)–(5) and Eq. (9), we know that velocity V is mainly controlled by fuel equivalence ratio Φ since the thrust T is directly affected by Φ; on the other hand, altitude h is mainly controlled by elevator angular deflection δ_e since δ_e directly affects pitch rate Q, and then affects pitch angle θ and flight-path γ, ultimately controls the change of h. Therefore, we can firstly decompose the AHV model into velocity subsystem [Eq. (1)] and altitude subsystem [Eqs. (2)–(5)], and then design the control law separately [46, 47].

For the velocity subsystem, the control objective is to make V steadily track its reference command V_{ref} by designing the control law Φ. Based on the research of Ref. [29], the velocity subsystem of AHV is further expressed as the following more general non-affine form.

$$\begin{cases} \dot{V} = F_V(V, \Phi) \\ y_V = V \end{cases} \tag{10}$$

where $F_V(V, \Phi)$ is a completely unknown continuously differentiable function; y_V is the output signal of the system (10).

At the same time, according to Ref. [45], the following reasonable assumption is given.

Assumption 1 For any $(V, \Phi) \in \Omega_V \times \mathbf{R}$, there is the following inequality established.

$$\frac{\partial F_V(V, \Phi)}{\partial \Phi} > 0 \tag{11}$$

where Ω_V is a controllable area.

For the altitude subsystem, the control target is to design the control law δ_e to make h stably track its reference command h_{ref}. Define the altitude tracking error as $\tilde{h} = h - h_{ref}$. According to the research conclusion of Ref. [29], the control target can be converted to ensure $\gamma \to \gamma_d$, where γ_d is the path angle command, which is taken as

$$\gamma_d = \arcsin\left(\frac{-k_{\gamma 1}\tilde{h} - k_{\gamma 2}\int_0^t \tilde{h}d\tau + \dot{h}_{ref}}{V}\right) \tag{12}$$

Similarly, according to the research conclusion in Ref. [29], the rest of the altitude subsystem [Eqs. (3)–(5)] is further expressed as the following more general non-affine form

$$\begin{cases} \dot{\gamma} = f_1(\gamma, \theta) \\ \dot{\theta} = Q \\ \dot{Q} = f_2(\boldsymbol{x}, \delta_e) \\ y_h = \gamma \end{cases} \tag{13}$$

where $\boldsymbol{x} = [\gamma, \theta, Q]^T$. Both $f_1(\gamma, \theta)$ and $f_2(\boldsymbol{x}, \delta_e)$ are completely unknown continuous differentiable functions; y_h is the output signal of system (13).

In order to facilitate subsequent control law design, the following assumption is also given according to Ref. [45].

Assumption 2 [48, 49] For any $(\boldsymbol{x}, \delta_e) \in \Omega_{\boldsymbol{x}} \times \mathbf{R}$, there is the following inequality established

$$\begin{cases} \dfrac{\partial f_1(\gamma,\theta)}{\partial\theta} > 0 \\ \dfrac{\partial f_2(\boldsymbol{x},\delta_e)}{\partial\delta_e} > 0 \end{cases} \tag{14}$$

where Ω_x is a controllable area.

In order to avoid the complex design process caused by the search for virtual control laws in the backstepping control, the following equivalent changes are made to the system (13).

Step 1 Let $z_1 = \gamma$, $z_2 = \dot{z}_1 = f_1(\gamma,\theta)$. According to Eq. (13), the time derivative of z_2 is derived as

$$\begin{aligned} \dot{z}_2 &= \frac{\partial f_1(\gamma,\theta)}{\partial\gamma}\dot{\gamma} + \frac{\partial f_1(\gamma,\theta)}{\partial\theta}\dot{\theta} \\ &= \frac{\partial f_1(\gamma,\theta)}{\partial\gamma} f_1(\gamma,\theta) + \frac{\partial f_1(\gamma,\theta)}{\partial\theta} Q \\ &\triangleq f_{h1}(\boldsymbol{x}) \end{aligned} \tag{15}$$

Step 2 Let $z_3 = \dot{z}_2 = f_{h1}(x)$. From Eq. (13), the time derivative of z_3 is derived as

$$\begin{aligned} \dot{z}_3 &= \frac{\partial f_{h1}(\boldsymbol{x})}{\partial\gamma}\dot{\gamma} + \frac{\partial f_{h1}(\boldsymbol{x})}{\partial\theta}\dot{\theta} + \frac{\partial f_{h1}(\boldsymbol{x})}{\partial Q}\dot{Q} \\ &= \frac{\partial f_{h1}(\boldsymbol{x})}{\partial\gamma} f_1(\gamma,\theta) + \frac{\partial f_{h1}(\boldsymbol{x})}{\partial\theta} Q + \frac{\partial f_{h1}(\boldsymbol{x})}{\partial Q} f_2(\boldsymbol{x},\delta_e) \\ &\triangleq f_{h2}(\boldsymbol{x},\delta_e) \end{aligned} \tag{16}$$

After the above model transformation, Eq. (13) is transformed to the following non-affine pure feedback model.

$$\begin{cases} \dot{z}_1 = z_2 \\ \dot{z}_2 = z_3 \\ \dot{z}_3 = f_{h2}(\boldsymbol{x},\delta_e) \\ y_h = z_1 \end{cases} \tag{17}$$

where $f_{h2}(\boldsymbol{x},\delta_e)$ is a completely unknown continuously differentiable function.

Remark 1 The existing references for the study of flexible AHV model control problems mostly use AHV as a strict feedback model with affine form (such as Refs. [37–43]), which do not reflect the non-affine form of the actual AHV model well. In this paper, AHV is regarded as a non-affine pure feedback model [Eqs. (10) and (13)], which better reflects the characteristics of actual AHV model, and the proposed non-affine control method is more reliable.

Remark 2 According to the value range of the rigid body state of the AHV flight envelope described in Ref. [45], Assumptions 1 and 2 are established.

Remark 3 From Eqs. (14)–(16), we can see

$$\begin{aligned} \frac{\partial f_{h2}(\boldsymbol{x},\delta_e)}{\partial\delta_e} &= \frac{\partial f_{h1}(\boldsymbol{x})}{\partial Q}\frac{\partial f_2(\boldsymbol{x},\delta_e)}{\partial\delta_e} \\ &= \frac{\partial f_1(\gamma,\theta)}{\partial\theta}\frac{\partial f_2(\boldsymbol{x},\delta_e)}{\partial\delta_e} > 0 \end{aligned} \tag{18}$$

2.3 RBFNN approximation

The RBFNN owns a simple structure, strong learning ability, and a global approximation ability for arbitrary nonlinear continuous functions [50]. It can be expressed as a mapping from input to output as follows

$$y = \boldsymbol{W}^{\mathrm{T}}\boldsymbol{h}(\boldsymbol{X}) \tag{19}$$

where $\boldsymbol{X} = [X_1, X_2, \ldots, X_n]^{\mathrm{T}} \in \mathbf{R}^n$ is the input vector; n stands for the dimension of the input vector; $\boldsymbol{W} = [w_1, w_2, \ldots, w_N]^{\mathrm{T}} \in \mathbf{R}^N$ is the weight vector; N represents the number of hidden layer nodes; $\boldsymbol{h}(\boldsymbol{X}) = [h_1(\boldsymbol{X}), h_2(\boldsymbol{X}), \cdots, h_N(\boldsymbol{X})]^{\mathrm{T}} \in \mathbf{R}^N$; $h_i(\boldsymbol{X})$ denotes activation function. Here, $h_i(\boldsymbol{X})$ is chosen as the following Gaussian function

$$h_i(\boldsymbol{X}) = \exp\left(-\frac{\|\boldsymbol{X}-\boldsymbol{c}_i\|^2}{2b_i^2}\right), i = 1, 2, \ldots, N \tag{20}$$

where $\boldsymbol{b} = [b_1, b_2, \ldots, b_N]^{\mathrm{T}} \in \mathbf{R}^N$; b_i is the width of the ith Gaussian function; $\boldsymbol{c} = [\boldsymbol{c}_1, \boldsymbol{c}_2, \ldots, \boldsymbol{c}_N] \in \mathbf{R}^{n\times N}$, $\boldsymbol{c}_i$ represents the center of the ith Gaussian function. It can be expressed as follows

$$\boldsymbol{c} = \begin{bmatrix} c_{11} & \cdots & c_{1N} \\ \vdots & \ddots & \vdots \\ c_{n1} & \cdots & c_{nN} \end{bmatrix}$$

For any unknown nonlinear continuous function $F(\boldsymbol{X})$, by using RBFNN and selecting enough nodes (selecting a sufficiently large N), there must be a set of ideal weight vector $\boldsymbol{W}^* = [w_1^*, w_2^*, \ldots, w_N^*]^{\mathrm{T}} \in \mathbf{R}^N$ to satisfy [50]

$$F(\boldsymbol{X}) = \boldsymbol{W}^{*\mathrm{T}} h(\boldsymbol{X}) + \mu, \quad |\mu| \le \mu_{\mathrm{M}} \tag{21}$$

where $\mu \in \mathbf{R}$ is approximation error; $\mu_{\mathrm{M}} \in \mathbf{R}^+$ represents the upper bound of approximation error. When taking N large enough, μ_{M} can be arbitrarily small.

Remark 4 Since $\exp(\bullet)$ is a strictly monotonically increasing and positive function, and $-||\boldsymbol{X} - \boldsymbol{c}_i||^2/(2b_i^2) \le 0$, there is $0 < h_i(\boldsymbol{X}) \le h_i(0) = 1$. Therefore, there must be a bounded constant $\bar{h} \in \mathbf{R}^+$ such that $||\boldsymbol{h}(\boldsymbol{X})|| \le \bar{h}$.

3 Adaptive neural controller design

This section presents the proposed adaptive neural control method for AHV with actuators multiple constraints. In Sects. 3.1 and 3.2, the adaptive neural controllers are designed for velocity subsystem and altitude subsystem, respectively. Then, in order to accurately estimate the high-order differential signals existing in the controller design process, finite-time-convergence-differentiator (FD) is introduced in Sect. 3.3.

3.1 Controller design for velocity subsystem

For the velocity subsystem [Eq. (10)], first define the velocity tracking error

$$\tilde{V} = V - V_{\mathrm{ref}} \tag{22}$$

where V_{ref} is velocity reference command.

Consider the actuator Φ constraint and define it as

$$\Phi = \begin{cases} \Phi_{\max}, \Phi_{\mathrm{c}} > \Phi_{\max} \\ \Phi_{\mathrm{c}}, \Phi_{\min} \le \Phi_{\mathrm{c}} \le \Phi_{\max} \\ \Phi_{\min}, \Phi_{\mathrm{c}} < \Phi_{\min} \end{cases} \tag{23}$$

where Φ_{c} is the ideal control law to be designed; $\Phi_{\min}$ and $\Phi_{\max}$ are the upper and lower bound of Φ, respectively.

In reality, the control input of the velocity subsystem (fuel equivalence ratio Φ) can change at a faster rate so that the phenomenon of actuator rate constraint is not easy to occur, thus only the amplitude constraint of actuator Φ is considered in this paper. However, for the altitude subsystem [Eq. (13)], when the elevator is in operation, its execution rate (the deflection rate of the elevator $\dot{\delta}_{\mathrm{e}}$) is affected by the physical structure and servo performance, so that it is subject to certain inherent constraints. Coupled with external disturbances such as gusts and turbulence, the deflection rate of the elevator will easily be constrained. Therefore, when designing the altitude subsystem controller in the following, both the amplitude and rate constraints of δ_{e} will be considered.

In order to deal with the actuator saturation problem mentioned above, design the following novel auxiliary error compensation system

$$\dot{\xi}_V = -\phi_V \mathrm{sgn}(\xi_V) \frac{\xi_V^2}{\xi_V^2 + \beta_V} + k_V(\Phi - \Phi_{\mathrm{c}}) \tag{24}$$

where $\phi_V, \beta_V, k_V \in \mathbf{R}^+$ are design parameters; ξ_V is the state variable of auxiliary system

Correct velocity tracking error $\tilde{V}$ to

$$e_V = \tilde{V} - \xi_V \tag{25}$$

Taking time derivative along Eq. (25) and combining Eqs. (10), (22) and (24), we obtain

$$\begin{aligned} \dot{e}_V &= \dot{\tilde{V}} - \dot{\xi}_V \\ &= F_V^*(V, \Phi) - \dot{V}_{\mathrm{ref}} + \phi_V \mathrm{sgn}(\xi_V) \frac{\xi_V^2}{\xi_V^2 + \beta_V} \\ &\quad + k_V \Phi_{\mathrm{c}} \end{aligned} \tag{26}$$

where $F_V^*(V, \Phi) = F_V(V, \Phi) - k_V \Phi$ is a completely unknown continuously differentiable function.

Design the ideal control law Φ_{c} as

$$\begin{cases} \Phi_{\mathrm{c}} = k_V^{-1}(\Phi_{\mathrm{c0}} - \Phi_{\mathrm{c1}}) \\ \Phi_{\mathrm{c0}} = -k_{V1} e_V - k_{V2} \int_0^t e_V \mathrm{d}\tau + \dot{V}_{\mathrm{ref}} \\ \qquad\quad - \phi_V \mathrm{sgn}(\xi_V) \xi_V^2/(\xi_V^2 + \beta_V) \end{cases} \tag{27}$$

where $k_{V1}, k_{V2} \in \mathbf{R}^+$ are design parameters; Φ_{c1} is an adaptive neural control law to be designed to counteract the influence of $F_V^*(V, \Phi)$.

In order to design Φ_{c1}, we use RBFNN to approximate $F_V^*(V, \Phi)$ and discuss it in two cases.

Case 1 If Φ is in saturation, there is $\Phi = \Phi_{\min}$ or $\Phi = \Phi_{\max}$. Since $\Phi_{\min}$ and $\Phi_{\max}$ are constants, $F_V^*(V, \Phi)$ can be considered as a function of V. Taking RBFNN's input vector as V can achieve an effective approximation to $F_V^*(V, \Phi)$.

Case 2 If Φ is not saturated, there is $\Phi = \Phi_{\mathrm{c}}$, then

$$F_V^*(V,\Phi)\triangleq F_V^*(V,\Phi_c) \tag{28}$$

For subsequent analysis, introduce the implicit function theorem [51]

Theorem 1 *Assume that implicit function* $L:\mathbf{R}^m\times\mathbf{R}^n\to\mathbf{R}^m$ *is continuously differentiable at each point* (x,y) *on open set* $Y\subset\mathbf{R}^m\times\mathbf{R}^n$. (x_0,y_0) *is the point where* $L(x_0,y_0)=0$ *is established in Y, and Jacobian matrix* $(\partial L/\partial x)(x_0,y_0)$ *is non-singular. Then, there is a neighborhood* $U\subset\mathbf{R}^m$ *of* x_0 *and a neighborhood* $G\subset\mathbf{R}^n$ *of* y_0, *so that for any* $y\in G$, *the equation* $L(x,y)=0$ *has a unique solution* $x\in U$, *and the solution can be expressed as* $x=g_0(y)$. *Here,* $g_0(\bullet)$ *is a continuously differentiable function on* $y=y_0$.

Remark 5 Theorem 1 shows that once implicit function $L(x, y)$ satisfies all conditions in the theorem, x can be expressed as a continuously differentiable function of y, and then there is $x=g_0(y)$. Therefore, when RBFNN is used to approximate $L(x, y)$, a satisfied approximation effect can be obtained only by using y instead of x as the input signal of the neural network. This is where the special meaning of the implicit function theorem lies.

Construct the following function

$$\begin{aligned}H_1(V,\Phi_{c0},\Phi_{c1})&\triangleq F_V^*(V,\Phi)-\Phi_{c1}\\&\triangleq F_V^*(V,\Phi_c)-\Phi_{c1}\\&=F_V^*(V,k_V{}^{-1}(\Phi_{c0}-\Phi_{c1}))-\Phi_{c1}\end{aligned} \tag{29}$$

To illustrate that $H_1(V,\Phi_{c0},\Phi_{c1})$ satisfies the implicit function theorem, the following theorem is firstly given.

Theorem 2 *If*

$$k_V>\frac{1}{2}\frac{\partial F_V(V,\Phi)}{\partial\Phi} \tag{30}$$

Then, for any $(V,\Phi_{c1})\in\Omega_V\times\mathbf{R}$, there is a controllable domain $\Omega_V\subset\mathbf{R}$ and a unique Φ_{c1}, so that

$$H_1(V,\Phi_{c0},\Phi_{c1})=0 \tag{31}$$

Proof According to Ref. [52], the sufficient condition for Φ_{c1} to exist is that the following inequality holds

$$\left|\frac{\partial F_V^*(V,\Phi_c)}{\partial\Phi_{c1}}\right|<1 \tag{32}$$

Combine Eqs. (11), (27), (28) and (30)

$$\begin{aligned}\left|\frac{\partial F_V^*(V,\Phi_c)}{\partial\Phi_{c1}}\right|&=\left|\frac{\partial F_V^*(V,\Phi)}{\partial\Phi_{c1}}\right|\\&=\left|\frac{\partial[F_V(V,\Phi)-k_V\Phi]}{\partial\Phi}\frac{\partial\Phi_c}{\partial\Phi_{c1}}\right|\\&=\left|\left[\frac{\partial F_V(V,\Phi)}{\partial\Phi}-k_V\right]\frac{1}{k_V}\right|\\&=\left|\frac{1}{k_V}\frac{\partial F_V(V,\Phi)}{\partial\Phi}-1\right|<1\end{aligned} \tag{33}$$

Therefore, Φ_{c1} exists. □

And then

$$\begin{aligned}\frac{\partial H_1(V,\Phi_{c0},\Phi_{c1})}{\partial\Phi_{c1}}&=\frac{\partial[F_V(V,\Phi)-k_V\Phi]}{\partial\Phi}\frac{\partial\Phi_c}{\partial\Phi_{c1}}-1\\&=\left[\frac{\partial F_V(V,\Phi)}{\partial\Phi}-k_V\right]\left(-\frac{1}{k_V}\right)-1\\&=-\frac{1}{k_V}\frac{\partial F_V(V,\Phi)}{\partial\Phi}\end{aligned} \tag{34}$$

Considering Eqs. (11) and (34), we get

$$\frac{\partial H_1(V,\Phi_{c0},\Phi_{c1})}{\partial\Phi_{c1}}<0 \tag{35}$$

Combining Theorems 1, 2 and Eq. (35), we can see that $H_1(V,\Phi_{c0},\Phi_{c1})$ satisfies the implicit function theorem. Therefore, Φ_{c1} can be seen as a function of Φ_{c0} and V, and further $F_V^*(V,\Phi)$ can be regarded as a function of Φ_{c0} and V.

Considering the above two conditions comprehensively, regardless of whether the actuator Φ is constrained, and when the input vectors of the RBFNN are taken as V and Φ_{c0}, an effective approximation to $F_V^*(V,\Phi)$ can be achieved, which can be expressed as follows.

$$F_V^*(V,\Phi)=\boldsymbol{W}_V^{*\mathrm{T}}\boldsymbol{h}(\boldsymbol{X}_1)+\varepsilon,|\varepsilon|\le\varepsilon_M \tag{36}$$

where $\boldsymbol{X}_1=[V,\Phi_{c0}]^{\mathrm{T}}\in\mathbf{R}^2$ is the input vector; $\boldsymbol{W}_V^{*\mathrm{T}}=[w_{V1}^*,w_{V2}^*,\ldots,w_{VN_1}^*]^{\mathrm{T}}\in\mathbf{R}^{N_1}$ is the weight vector; N_1 represents the number of hidden layer nodes; ε and ε_M stand for approximation errors and its upper bounds; $\boldsymbol{h}(\boldsymbol{X}_1)=[h_1(\boldsymbol{X}_1),\ldots h_{N_1}(\boldsymbol{X}_1)]^{\mathrm{T}}\in\mathbf{R}^{N_1}$, where $h_i(\boldsymbol{X}_1)$

is the activation function, here it is chosen as the Gaussian function.

The following is based on the minimum learning parameter algorithm (MLP) idea and adaptively adjusting the norm of the RBFNN's weight vector.

Define $\omega_V = \left\|W_V^*\right\|^2$ and design Φ_{c1} as

$$\Phi_{c1} = \frac{1}{2} e_V \hat{\omega}_V \boldsymbol{h}^{\mathrm{T}}(\boldsymbol{X}_1)\boldsymbol{h}(\boldsymbol{X}_1) \tag{37}$$

where $\hat{\omega}_V$ is the estimation of ω_V; and design its adaptive law as

$$\dot{\hat{\omega}}_V = \frac{\mu_V}{2} e_V^2 \boldsymbol{h}^{\mathrm{T}}(\boldsymbol{X}_1)\boldsymbol{h}(\boldsymbol{X}_1) - 2\hat{\omega}_V \tag{38}$$

where $\mu_V \in \mathbf{R}^+$ is design parameter.

3.2 Controller design for altitude subsystem

For the altitude subsystem (13), define flight-path tracking error $\tilde{\gamma}$ and error function E

$$\begin{cases} \tilde{\gamma} = \gamma - \gamma_{\mathrm{d}} = z_1 - \gamma_{\mathrm{d}} \\ E = \left(\dfrac{\mathrm{d}}{\mathrm{d}t} + \lambda\right)^3 \displaystyle\int_0^t \tilde{\gamma}\mathrm{d}\tau \\ \quad = \dddot{\tilde{\gamma}} + 3\lambda\ddot{\tilde{\gamma}} + 3\lambda^2\dot{\tilde{\gamma}} + \lambda^3 \displaystyle\int_0^t \tilde{\gamma}\mathrm{d}\tau \end{cases} \tag{39}$$

where $\lambda \in \mathbf{R}^+$ is design parameter. Since $(s+\lambda)^3$ is a Hurwitz polynomial, when E is bounded, $\tilde{\gamma}$ must be bounded.

Considering that elevator angular deflection δ_{e} is constrained in both amplitude and rate, define it as

$$\delta_{\mathrm{e}} = \begin{cases} \delta_{\mathrm{e}\max}, \delta_{\mathrm{ec}} > \delta_{\mathrm{e}\max} \\ \delta_{\mathrm{ec}}, \delta_{\mathrm{e}\min} \le \delta_{\mathrm{ec}} \le \delta_{\mathrm{e}\max} \\ \delta_{\mathrm{e}\min}, \delta_{\mathrm{ec}} < \delta_{\mathrm{e}\min} \end{cases} \tag{40}$$

$$\omega_{\mathrm{e}} = \begin{cases} \omega_{\mathrm{e}\max}, \omega_{\mathrm{ec}} > \omega_{\mathrm{e}\max} \\ \omega_{\mathrm{ec}}, \omega_{\mathrm{e}\min} \le \omega_{\mathrm{ec}} \le \omega_{\mathrm{e}\max} \\ \omega_{\mathrm{e}\min}, \omega_{\mathrm{ec}} < \omega_{\mathrm{e}\min} \end{cases} \tag{41}$$

where $\omega_{\mathrm{e}} = \dot{\delta}_{\mathrm{e}}$ is the deflection rate of the elevator; δ_{ec} and ω_{ec} are the ideal control laws to be designed; $\delta_{\mathrm{e}\min}$ and $\delta_{\mathrm{e}\max}(\delta_{\mathrm{e}\max} = -\delta_{\mathrm{e}\min} > 0)$are the upper and lower bound of δ_{e}, respectively; $\omega_{\mathrm{e}\min}$ and $\omega_{\mathrm{e}\max}(\omega_{\mathrm{e}\max} = -\omega_{\mathrm{e}\min} > 0)$ stand for the upper and lower bound of ω_{e}, respectively.

In order to deal with the problem of amplitude saturation of δ_{e} [Eq. (40)], a new high-order auxiliary system is designed as follows

$$\begin{cases} \dot{\xi}_{h1} = \xi_{h2} \\ \dot{\xi}_{h2} = \xi_{h3} \\ \dot{\xi}_{h3} = -\phi_{h1}\mathrm{sgn}(\xi_{h3})\dfrac{\xi_{h1}^2}{\xi_{h1}^2 + \beta_{h1}} - \phi_{h2}\dfrac{\xi_{h2}^2}{\xi_{h2}^2 + \beta_{h2}} \\ \qquad - \phi_{h3}\mathrm{sgn}(\xi_{h3})\dfrac{\xi_{h3}^2}{\xi_{h3}^2 + \beta_{h3}} + k_h(\delta_{\mathrm{e}} - \delta_{\mathrm{ec}}) \end{cases} \tag{42}$$

where $\xi_{h1}, \xi_{h2}, \xi_{h3} \in \mathbf{R}$ are the state variables of auxiliary system; ϕ_{h1}, ϕ_{h2}, ϕ_{h3}, β_{h1}, β_{h2}, β_{h3} and $k_h \in \mathbf{R}^+$ are design parameters.

Correct $\tilde{\gamma}$ and E as

$$\begin{cases} e_\gamma = \tilde{\gamma} - \xi_{h1} = z_1 - \gamma_{\mathrm{d}} - \xi_{h1} \\ E' = \left(\dfrac{\mathrm{d}}{\mathrm{d}t} + \lambda\right)^3 \displaystyle\int_0^t e_\gamma \mathrm{d}\tau \\ \quad = \dddot{e}_\gamma + 3\lambda\ddot{e}_\gamma + 3\lambda^2\dot{e}_\gamma + \lambda^3 \displaystyle\int_0^t e_\gamma \mathrm{d}\tau \end{cases} \tag{43}$$

The first three order derivatives of e_γ are

$$\begin{cases} \dot{e}_\gamma = \dot{z}_1 - \dot{\gamma}_{\mathrm{d}} - \dot{\xi}_{h1} = z_2 - \dot{\gamma}_{\mathrm{d}} - \xi_{h2} \\ \ddot{e}_\gamma = \dot{z}_2 - \ddot{\gamma}_{\mathrm{d}} - \dot{\xi}_{h2} = z_3 - \ddot{\gamma}_{\mathrm{d}} - \xi_{h3} \\ \dddot{e}_\gamma = \dot{z}_3 - \dddot{\gamma}_{\mathrm{d}} - \dot{\xi}_{h3} = f_{h2}(\boldsymbol{x}, \delta_{\mathrm{e}}) - k_h\delta_{\mathrm{e}} + k_h\delta_{\mathrm{ec}} - \dddot{\gamma}_{\mathrm{d}} \\ \qquad + \dfrac{\phi_{h1}\mathrm{sgn}(\xi_{h3})\xi_{h1}^2}{\xi_{h1}^2 + \beta_{h1}} + \dfrac{\phi_{h2}\xi_{h2}^2}{\xi_{h2}^2 + \beta_{h2}} + \dfrac{\phi_{h3}\mathrm{sgn}(\xi_{h3})\xi_{h3}^2}{\xi_{h3}^2 + \beta_{h3}} \\ \quad = F_h(\boldsymbol{x}, \delta_{\mathrm{e}}) + k_h\delta_{\mathrm{ec}} - \dddot{\gamma}_{\mathrm{d}} + \dfrac{\phi_{h1}\mathrm{sgn}(\xi_{h3})\xi_{h1}^2}{\xi_{h1}^2 + \beta_{h1}} \\ \qquad + \dfrac{\phi_{h2}\xi_{h2}^2}{\xi_{h2}^2 + \beta_{h2}} + \dfrac{\phi_{h3}\mathrm{sgn}(\xi_{h3})\xi_{h3}^2}{\xi_{h3}^2 + \beta_{h3}} \end{cases} \tag{44}$$

where $F_h(\boldsymbol{x}, \delta_{\mathrm{e}}) = f_{h2}(\boldsymbol{x}, \delta_{\mathrm{e}}) - k_h\delta_{\mathrm{e}}$.

Taking time derivative along E' and combining Eqs. (43) and (44), we have

$$\begin{aligned}\dot{E}' &= \dddot{e}_\gamma + 3\lambda\ddot{e}_\gamma + 3\lambda^2\dot{e}_\gamma + \lambda^3 e_\gamma \\ &= F_h(\boldsymbol{x},\delta_e) + k_h\delta_{ec} - \dddot{\gamma}_d + \frac{\phi_{h1}\mathrm{sgn}(\xi_{h3})\xi_{h1}^2}{\xi_{h1}^2+\beta_{h1}} \\ &\quad + \frac{\phi_{h2}\xi_{h2}^2}{\xi_{h2}^2+\beta_{h2}} + \frac{\phi_{h3}\mathrm{sgn}(\xi_{h3})\xi_{h3}^2}{\xi_{h3}^2+\beta_{h3}} + 3\lambda\ddot{e}_\gamma \\ &\quad + 3\lambda^2\dot{e}_\gamma + \lambda^3 e_\gamma\end{aligned} \tag{45}$$

Through the previous model conversion process, we can see $z_2 = \dot{\gamma}$ and $z_3 = \ddot{\gamma}$. In order to avoid the "explosion of terms" problem, the FD will be used to accurately estimate the differential signal. Use γ as the FD's input signal (take $n = 4$) to get the estimations of z_2 and z_3, denoted as $\hat{z}_2$ and $\hat{z}_3$; Similarly, using γ_d as the FD's input signal (takes $n = 4$), we can get estimations for $\dot{\gamma}_d$, $\ddot{\gamma}_d$, and $\dddot{\gamma}_d$, represented as $\dot{\hat{\gamma}}_d$, $\ddot{\hat{\gamma}}_d$, and $\dddot{\hat{\gamma}}_d$, respectively.

Therefore, the estimate of the first three derivatives of e_γ can be expressed as

$$\begin{cases} \dot{\hat{e}}_\gamma = \hat{z}_2 - \dot{\hat{\gamma}}_d - \xi_{h2} \\ \ddot{\hat{e}}_\gamma = \hat{z}_3 - \ddot{\hat{\gamma}}_d - \xi_{h3} \\ \dddot{\hat{e}}_\gamma = F_h(\boldsymbol{x},\delta_e) + k_h\delta_{ec} - \dddot{\gamma}_d + \dfrac{\phi_{h1}\mathrm{sgn}(\xi_{h3})\xi_{h1}^2}{\xi_{h1}^2+\beta_{h1}} \\ \qquad + \dfrac{\phi_{h2}\xi_{h2}^2}{\xi_{h2}^2+\beta_{h2}} + \dfrac{\phi_{h3}\mathrm{sgn}(\xi_{h3})\xi_{h3}^2}{\xi_{h3}^2+\beta_{h3}} \end{cases} \tag{46}$$

Combining Eqs. (43), (45) and (46), the estimations of E' and $\dot{E}'$ are

$$\hat{E}' = \ddot{\hat{e}}_\gamma + 3\lambda\dot{\hat{e}}_\gamma + 3\lambda^2 e_\gamma + \lambda^3\int_0^t e_\gamma \mathrm{d}\tau \tag{47}$$

$$\begin{aligned}\dot{\hat{E}}' &= F_h(\boldsymbol{x},\delta_e) + k_h\delta_{ec} - \dddot{\gamma}_d + \frac{\phi_{h1}\mathrm{sgn}(\xi_{h3})\xi_{h1}^2}{\xi_{h1}^2+\beta_{h1}} \\ &\quad + \frac{\phi_{h2}\xi_{h2}^2}{\xi_{h2}^2+\beta_{h2}} + \frac{\phi_{h3}\mathrm{sgn}(\xi_{h3})\xi_{h3}^2}{\xi_{h3}^2+\beta_{h3}} + 3\lambda\ddot{\hat{e}}_\gamma \\ &\quad + 3\lambda^2\dot{\hat{e}}_\gamma + \lambda^3 e_\gamma\end{aligned} \tag{48}$$

Design the ideal control law δ_{ec} as

$$\begin{cases} \delta_{ec} = k_h^{-1}(\delta_{ec0} - \delta_{ec1}) \\ \delta_{ec0} = -k_{h1}\hat{E}' + \dddot{\hat{\gamma}}_d - 3\lambda\ddot{\hat{e}}_\gamma - 3\lambda^2\dot{\hat{e}}_\gamma \\ \qquad - \lambda^3 e_\gamma - \dfrac{\phi_{h1}\mathrm{sgn}(\xi_{h3})\xi_{h1}^2}{\xi_{h1}^2+\beta_{h1}} - \dfrac{\phi_{h2}\xi_{h2}^2}{\xi_{h2}^2+\beta_{h2}} \\ \qquad - \dfrac{\phi_{h3}\mathrm{sgn}(\xi_{h3})\xi_{h3}^2}{\xi_{h3}^2+\beta_{h3}} \end{cases} \tag{49}$$

where $k_{h1} \in \mathbf{R}^+$ is design parameter. δ_{ec1} is the neural control law to be designed to counteract the influence of the unknown function $F_h(\boldsymbol{x},\delta_e)$.

Using RBFNN to approximate $F_h(\boldsymbol{x},\delta_e)$, the following two situations are discussed.

Case 1 If δ_e is in saturation, there is $\delta_e = \delta_{emin}$ or $\delta_e = \delta_{emax}$. Since both δ_{emin} and δ_{emax} are constants, $F_h(\boldsymbol{x},\delta_e)$ can be regarded as a function of $\boldsymbol{x}$. Furthermore, using $\boldsymbol{x}$ as the input vector of RBFNN can achieve an effective approximation to $F_h(\boldsymbol{x},\delta_e)$.

Case 2 If δ_e is not saturated, there is $\delta_e = \delta_{ec}$, and then there is

$$F_h(\boldsymbol{x},\delta_e) \triangleq F_h(\boldsymbol{x},\delta_{ec}) \tag{50}$$

Construct the following function

$$\begin{aligned}H_2(\boldsymbol{x},\delta_{ec0},\delta_{ec1}) &\triangleq F_h(\boldsymbol{x},\delta_e) - \delta_{ec1} \\ &\triangleq F_h(\boldsymbol{x},\delta_{ec}) - \delta_{ec1} \\ &= F_h(\boldsymbol{x},k_h^{-1}(\delta_{ec0}-\delta_{ec1})) - \delta_{ec1}\end{aligned} \tag{51}$$

Similar to the analysis process of Theorems 2, 3 is given here, and the proof process is not repeated.

Theorem 3 *If*

$$k_h > \frac{1}{2}\frac{\partial f_{h2}(\boldsymbol{x},\delta_e)}{\partial\delta_e} \tag{52}$$

For any $(\boldsymbol{x},\delta_{ec0}) \in \Omega_x \times \mathbf{R}$, there is a controllable domain $\Omega_x \subset \mathbf{R}^3$ and a unique δ_{ec1}, such that

$$H_2(\boldsymbol{x},\delta_{ec0},\delta_{ec1}) = 0 \tag{53}$$

Similar to Eq. (34), there is

$$\frac{\partial H_2(\boldsymbol{x},\delta_{ec0},\delta_{ec1})}{\partial\delta_{ec1}} < 0 \tag{54}$$

According to Theorem 3 and Eq. (54), $H_2(\boldsymbol{x}, \delta_{ec0}, \delta_{ec1})$ satisfies the implicit function theorem. Then, δ_{ec1} can be regarded as a function of $\boldsymbol{x}$ and δ_{ec0}, and further $F_h(\boldsymbol{x}, \delta_e)$ can be regarded as a function of x and δ_{ec0}.

Considering the above two cases comprehensively, if $\boldsymbol{x}$ and δ_{ec0} are used as the input vectors of the RBFNN, an effective approximation to $F_h(\boldsymbol{x}, \delta_e)$ can be achieved, which can be expressed as

$$F_h(\boldsymbol{x}, \delta_e) = \boldsymbol{W}_h^{*\mathrm{T}} \boldsymbol{h}(\boldsymbol{X}_2) + \iota, |\iota| \le \iota_M \tag{55}$$

where $\boldsymbol{X}_2 = [\boldsymbol{x}^{\mathrm{T}}, \ \delta_{ec0}]^{\mathrm{T}} \in \mathbf{R}^4$ is the input vector; $\boldsymbol{W}_h^{*\mathrm{T}} = [w_{h1}^*, w_{h2}^*, \ldots, w_{hN_2}^*]^{\mathrm{T}} \in \mathbf{R}^{N_2}$ is the weight vector; N_2 represents the number of hidden layer nodes; ι and ι_M stand for approximation errors and its upper bounds; $\boldsymbol{h}(\boldsymbol{X}_2) = [h_1(\boldsymbol{X}_2), \ldots h_{N_1}(\boldsymbol{X}_2)]^{\mathrm{T}} \in \mathbf{R}^{N_2}$, where $h_i(\boldsymbol{X}_2)$ is the activation function, here it is chosen as the Gaussian function.

Define $\omega_h = \left\| \boldsymbol{W}_h^* \right\|^2$, design δ_{ec1} as

$$\delta_{ec1} = \frac{1}{2} \hat{E}' \hat{\omega}_h \boldsymbol{h}^{\mathrm{T}}(\boldsymbol{X}_2) \boldsymbol{h}(\boldsymbol{X}_2) \tag{56}$$

where $\hat{\omega}_h$ is the estimation of ω_h; Its adaptive law is designed to

$$\dot{\hat{\omega}}_h = \frac{\mu_h}{2} \hat{E}'^2 \boldsymbol{h}^{\mathrm{T}}(\boldsymbol{X}_2) \boldsymbol{h}(\boldsymbol{X}_2) - 2\hat{\omega}_h \tag{57}$$

where $\mu_h \in \mathbf{R}^+$ is design parameter.

Through the above analysis, under the condition that the amplitude of the elevator angular deflection is constrained, we have obtained the control law δ_e [Eqs. (40), (49) and (56)] that needs to be executed. However, considering the saturation of the deflection rate of the elevator [Eq. (41)], the above δ_e may not be effectively executed, resulting in the instability of the closed-loop control system. The following is divided into three cases.

Case 1 If δ_e is in saturation, there is $\delta_e = \delta_{emax}$ or $\delta_e = \delta_{emin}$. In this case, there is $\omega_e = \dot{\delta}_e = 0$, the deflection rate of the elevator is not saturated, and the control law δ_e can be effectively executed.

Case 2 If δ_e is not in saturation, there is $\delta_{emin} \le \delta_e = \delta_{ec} \le \delta_{emax}$. And if $\omega_{emin} < \dot{\delta}_e < \omega_{emax}$, then δ_e can be effectively executed.

Case 3 If $\delta_{emin} \le \delta_e = \delta_{ec} \le \delta_{emax}$, and if $\dot{\delta}_{ec} > \omega_{emax}$ or $\dot{\delta}_{ec} < \omega_{emin}$, then δ_e cannot be effectively executed.

In order to avoid the instability of the closed-loop control system caused by δ_e being unable to be executed, the ideal control law δ_{ec} needs to be corrected. The corrected control law is designed as follows

$$\delta_{ec}^* = \begin{cases} \delta_{ec}, & \text{Case 1 and Case 2} \\ \delta'_{ec}, & \text{Case 3} \end{cases} \tag{58}$$

For Case 3, define the execution error of δ_e

$$\tilde{\delta}_e = \delta'_{ec} - \delta_{ec} \tag{59}$$

where δ'_{ec} stands for executable δ_e. Its first derivative $\dot{\delta}'_{ec} = \omega_e$ is the actual deflection rate of the elevator.

Considering that the deflection rate of the elevator is constrained, design the following auxiliary system

$$\dot{\xi}_\delta = -\phi_\delta \mathrm{sgn}(\xi_\delta) \frac{\xi_\delta^2}{\xi_\delta^2 + \beta_\delta} + (\omega_e - \omega_{ec}) \tag{60}$$

where $\phi_\delta, \beta_\delta \in \mathbf{R}^+$ are design parameters; ξ_δ is the state variable of auxiliary system.

Correct $\tilde{\delta}_e$ to

$$e_\delta = \tilde{\delta}_e - \xi_\delta \tag{61}$$

Take time derivative along Eq. (61)

$$\begin{aligned} \dot{e}_\delta &= \dot{\tilde{\delta}}_e - \dot{\xi}_\delta \\ &= \omega_e - \dot{\delta}_{ec} - \omega_e + \omega_{ec} + \phi_\delta \mathrm{sgn}(\xi_\delta) \frac{\xi_\delta^2}{\xi_\delta^2 + \beta_\delta} \\ &= \omega_{ec} - \dot{\delta}_{ec} + \phi_\delta \mathrm{sgn}(\xi_\delta) \frac{\xi_\delta^2}{\xi_\delta^2 + \beta_\delta} \end{aligned} \tag{62}$$

Design the ideal control law ω_{ec} as

$$\omega_{ec} = -k_{\delta 1} e_\delta - k_{\delta 2} \int_0^t e_\delta \mathrm{d}\tau + \dot{\hat{\delta}}_{ec} - \frac{\phi_\delta \mathrm{sgn}(\xi_\delta) \xi_\delta^2}{\xi_\delta^2 + \beta_\delta} \tag{63}$$

where $k_{\delta 1}, k_{\delta 2} \in \mathbf{R}^+$ are design parameters; $\dot{\hat{\delta}}_{ec}$ is the estimation of $\dot{\delta}_{ec}$, which can be acquired using FD below.

Combining Eqs. (41) and (63), the actual ω_e can be obtained so that δ'_{ec} can be expressed as

$$\delta'_{\mathrm{ec}} = \int_0^t \omega_{\mathrm{e}} \mathrm{d}\tau \tag{64}$$

3.3 Finite-time-convergence-differentiator (FD)

Consider the following FD [53]

$$\begin{cases} \dot{x}_1 = x_2 \\ \dot{x}_2 = x_3 \\ \quad \vdots \\ \dot{x}_{n-1} = x_n \\ \dot{x}_n = R^n \left[-a_1 \arctan(x_1 - \upsilon(t)) - a_2 \arctan\left(\dfrac{x_2}{R}\right) \right. \\ \qquad \left. - \cdots - a_n \arctan\left(\dfrac{x_n}{R^{n-1}}\right) \right] \end{cases} \tag{65}$$

where $R, a_i (i = 1, 2, \ldots, n) \in \mathbf{R}^+$ are design parameters;$x_i (i = 1, 2, \ldots, n)$ are the state variables of system; x_1 is the estimation of $\upsilon(t)$; $x_i (i = 2, 3, \ldots, n)$ stands for the estimation of the $(i-1)$th derivative of $\upsilon(t)$.

According to Ref. [53], for the system (65), there are $\phi > 0$ and $\imath\phi > n$ so that

$$x_i - \upsilon^{(i-1)}(t) = O\left(\left(\frac{1}{R}\right)^{\imath\phi - i + 1} \right), i = 1, 2, \ldots, n \tag{66}$$

where $O((1/R)^{\imath\phi - i + 1})$ represents the approximation of $(1/R)^{\imath\phi - i + 1}$ order between x_i and $\upsilon^{(i-1)}(t)$.

Therefore, there must be a bounded constant $v_{iM} > 0$

$$\left| x_i - \upsilon^{(i-1)}(t) \right| \le v_{iM} \tag{67}$$

The above FD is used to estimate z_2, z_3, $\dot{\gamma}_{\mathrm{d}}$, $\ddot{\gamma}_{\mathrm{d}}$, $\dddot{\gamma}_{\mathrm{d}}$ and $\dot{\delta}_{\mathrm{ec}}$.

$$\begin{cases} \dot{\hat{z}}_1 = \hat{z}_2 \\ \dot{\hat{z}}_2 = \hat{z}_3 \\ \dot{\hat{z}}_3 = \hat{z}_4 \\ \dot{\hat{z}}_4 = R_1^4 \left[-a_{11} \arctan(\hat{z}_1 - \gamma) - a_{12} \arctan\left(\dfrac{\hat{z}_2}{R_1}\right) \right. \\ \qquad \left. - a_{13} \arctan\left(\dfrac{\hat{z}_3}{R_1^2}\right) - a_{14} \arctan\left(\dfrac{\hat{z}_4}{R_1^3}\right) \right] \end{cases} \tag{68}$$

$$\begin{cases} (\hat{\gamma}_{\mathrm{d}})' = \dot{\hat{\gamma}}_{\mathrm{d}} \\ (\dot{\hat{\gamma}}_{\mathrm{d}})' = \ddot{\hat{\gamma}}_{\mathrm{d}} \\ (\ddot{\hat{\gamma}}_{\mathrm{d}})' = \dddot{\hat{\gamma}}_{\mathrm{d}} \\ (\dddot{\hat{\gamma}}_{\mathrm{d}})' = R_2^4 \left[-a_{21} \arctan(\hat{\gamma}_{\mathrm{d}} - \gamma_{\mathrm{d}}) - a_{22} \arctan\left(\dfrac{\dot{\hat{\gamma}}_{\mathrm{d}}}{R_2}\right) \right. \\ \qquad \left. - a_{23} \arctan\left(\dfrac{\ddot{\hat{\gamma}}_{\mathrm{d}}}{R_1^2}\right) - a_{24} \arctan\left(\dfrac{\dddot{\hat{\gamma}}_{\mathrm{d}}}{R_2^3}\right) \right] \end{cases} \tag{69}$$

$$\begin{cases} (\hat{\delta}_{\mathrm{ec}})' = \dot{\hat{\delta}}_{\mathrm{ec}} \\ (\dot{\hat{\delta}}_{\mathrm{ec}})' = R_3^2 \left[-a_{31} \arctan\left(\hat{\delta}_{\mathrm{ec}} - \delta_{\mathrm{ec}}\right) - a_{32} \arctan\left(\dfrac{\dot{\hat{\delta}}_{\mathrm{ec}}}{R_3}\right) \right] \end{cases} \tag{70}$$

where $R_i, a_{ij} (i = 1, 2, 3; j = 1, 2, 3, 4) \in \mathbf{R}^+$ are design parameters; $(*)'$ represents the first derivative of $*$; $\hat{z}_1$, $\hat{z}_2$, $\hat{z}_3$ and $\hat{z}_4$ represent the estimations of $z_1(\gamma)$, $z_2(\dot{\gamma})$, $z_3(\ddot{\gamma})$ and $z_4(\dddot{\gamma})$, respectively;$\hat{\gamma}_{\mathrm{d}}$, $\dot{\hat{\gamma}}_{\mathrm{d}}$, $\ddot{\hat{\gamma}}_{\mathrm{d}}$ and $\dddot{\hat{\gamma}}_{\mathrm{d}}$ stand for the estimations of γ_{d}, $\dot{\gamma}_{\mathrm{d}}$, $\ddot{\gamma}_{\mathrm{d}}$ and $\dddot{\gamma}_{\mathrm{d}}$, respectively; $\hat{\delta}_{\mathrm{ec}}$ and $\dot{\hat{\delta}}_{\mathrm{ec}}$ are the estimations of δ_{ec} and $\dot{\delta}_{\mathrm{ec}}$, respectively.

The structure of the proposed control scheme is shown in Fig. 2.

4 Stability analysis

This section analyzes the stability of the proposed control method. In Sect. 4.1, the proof of Theorem 4 shows that the velocity subsystem is stable and velocity tracking error $\tilde{V}$ is bounded. And in Sect. 4.2,

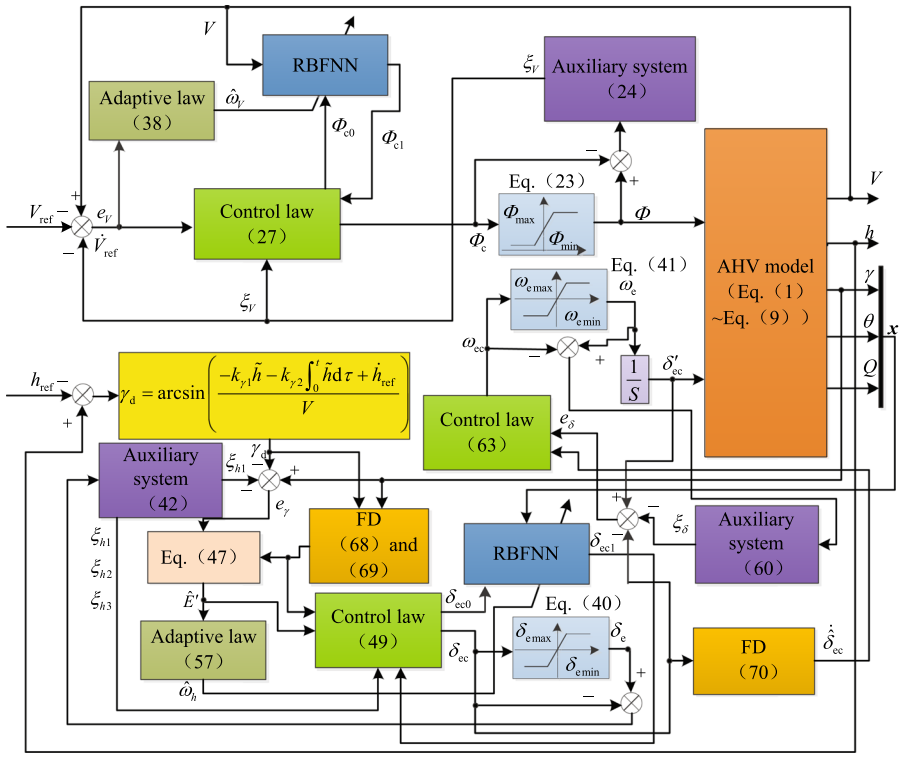

Fig. 2 The structure of the proposed control scheme

the stability of the altitude subsystem and the boundedness of path angle tracking error $\tilde{\gamma}$ are proved by Theorem 5.

4.1 Stability analysis for velocity subsystem

Theorem 4 *For the velocity subsystem of AHV* [*Eq.* (10)], *considering the saturation of actuator* Φ [*Eq.* (23)], *and using the designed control laws* (27), (37) *and the adaptive law* (38), *the closed-loop control system is semi-globally uniformly ultimately stable, and the velocity tracking error* $\tilde{V}$ *is bounded.*

Proof The proof process can be divided into two steps.

Step 1. Prove that e_V is bounded.

Define the estimation error of ω_V

$$\tilde{\omega}_V = \hat{\omega}_V - \omega_V \tag{71}$$

Substituting Eqs. (27), (36) and (37) into Eq. (26), we get

$$\begin{aligned}\dot{e}_V &= \Phi_{c0} - \Phi_{c1} + \boldsymbol{W}_V^{*\mathrm{T}}\boldsymbol{h}(\boldsymbol{X}_1) + \varepsilon - \dot{V}_{\mathrm{ref}} + \frac{\phi_V \mathrm{sgn}(\xi_V)\xi_V^2}{\xi_V^2 + \beta_V} \\ &= -k_{V1}e_V - k_{V2}\int_0^t e_V \mathrm{d}\tau - \frac{1}{2}e_V\hat{\omega}_V\boldsymbol{h}^{\mathrm{T}}(\boldsymbol{X}_1)\boldsymbol{h}(\boldsymbol{X}_1) \\ &\quad + \boldsymbol{W}_V^{*\mathrm{T}}\boldsymbol{h}(\boldsymbol{X}_1) + \varepsilon\end{aligned} \tag{72}$$

Choose the following Lyapunov function

$$W_V = \frac{1}{2}e_V^2 + \frac{1}{2}k_{V2}\left(\int_0^t e_V \mathrm{d}\tau\right)^2 + \frac{\tilde{\omega}_V^2}{2\mu_V} \tag{73}$$

Taking time derivative along Eq. (73) and invoking Eqs. (38) and (72), we have

$$\begin{aligned}\dot{W}_V &= e_V\dot{e}_V + k_{V2}e_V\int_0^t e_V\mathrm{d}\tau + \frac{\tilde{\omega}_V\dot{\hat{\omega}}_V}{\mu_V}\\ &= e_V\Big[-k_{V1}e_V - k_{V2}\int_0^t e_V\mathrm{d}\tau\\ &\quad -\frac{1}{2}e_V\hat{\omega}_V\boldsymbol{h}^{\mathrm{T}}(\boldsymbol{X}_1)\boldsymbol{h}(\boldsymbol{X}_1) + \boldsymbol{W}_V^{*\mathrm{T}}\boldsymbol{h}(\boldsymbol{X}_1) + \varepsilon\Big]\\ &\quad + k_{V2}e_V\int_0^t e_V\mathrm{d}\tau + \frac{\tilde{\omega}_V}{\mu_V}\Big[\frac{\mu_V}{2}e_V^2\boldsymbol{h}^{\mathrm{T}}(\boldsymbol{X}_1)\boldsymbol{h}(\boldsymbol{X}_1) - 2\hat{\omega}_V\Big]\\ &= -k_{V1}e_V^2 - \frac{1}{2}e_V^2\omega_V\boldsymbol{h}^{\mathrm{T}}(\boldsymbol{X}_1)\boldsymbol{h}(\boldsymbol{X}_1) +\\ &\quad e_V\boldsymbol{W}_V^{*\mathrm{T}}\boldsymbol{h}(\boldsymbol{X}_1) + e_V\varepsilon - \frac{2\tilde{\omega}_V\hat{\omega}_V}{\mu_V}\end{aligned} \tag{74}$$

Since

$$e_V\boldsymbol{W}_V^{*\mathrm{T}}\boldsymbol{h}(\boldsymbol{X}_1) \le \frac{{e_V}^2}{2}\left\|\boldsymbol{W}_V^{*\mathrm{T}}\boldsymbol{h}(\boldsymbol{X}_1)\right\|^2 + \frac{1}{2}$$

$$e_V\varepsilon \le \frac{{e_V}^2}{4} + \varepsilon_M^2, \quad 2\tilde{\omega}_V\hat{\omega}_V \ge \tilde{\omega}_V^2 - \omega_V^2$$

According to Cauchy–Schwarz inequality

$$\left\|\boldsymbol{W}_V^{*\mathrm{T}}\boldsymbol{h}(\boldsymbol{X}_1)\right\| \le \left\|\boldsymbol{W}_V^*\right\|\|\boldsymbol{h}(\boldsymbol{X}_1)\|$$

And then

$$\begin{aligned}e_V\boldsymbol{W}_V^{*\mathrm{T}}\boldsymbol{h}(\boldsymbol{X}_1) &\le \frac{{e_V}^2}{2}\left\|\boldsymbol{W}_V^*\right\|^2\|\boldsymbol{h}(\boldsymbol{X}_1)\|^2 + \frac{1}{2}\\ &= \frac{{e_V}^2}{2}\omega_V\boldsymbol{h}^{\mathrm{T}}(\boldsymbol{X}_1)\boldsymbol{h}(\boldsymbol{X}_1) + \frac{1}{2}\end{aligned}$$

At this point, Eq. (74) becomes

$$\dot{W}_V \le -\left(k_{V1} - \frac{1}{4}\right)e_V^2 - \frac{\tilde{\omega}_V^2}{\mu_V} + \frac{1}{2} + \varepsilon_M^2 + \frac{\omega_V^2}{\mu_V} \tag{75}$$

Let $k_{V1} > 1/4$ and define the following compact sets

$$\begin{aligned}\Omega_{e_V} &= \left\{e_V\middle||e_V| \le \sqrt{\left(\frac{1}{2} + \varepsilon_M^2 + \frac{\omega_V^2}{\mu_V}\right)\Big/\left(k_{V1} - \frac{1}{4}\right)}\right\}\\ \Omega_{\tilde{\omega}_V} &= \left\{\tilde{\omega}_V\middle||\tilde{\omega}_V| \le \sqrt{\left(\frac{1}{2} + \varepsilon_M^2 + \frac{\omega_V^2}{\mu_V}\right)\Big/\left(\frac{1}{\mu_V}\right)}\right\}\end{aligned} \tag{76}$$

If $e_V \notin \Omega_{e_V}$ or $\tilde{\omega}_V \notin \Omega_{\tilde{\omega}_V}$, then $\dot{W}_V < 0$, so the closed-loop control system is semi-globally uniformly ultimately stable. The errors e_V and $\tilde{\omega}_V$ are semi-globally uniformly ultimately bounded, and eventually converge into compact sets Ω_{e_V} and $\Omega_{\tilde{\omega}_V}$, respectively. By selecting k_{V1} sufficiently large and μ_V sufficiently small, the compact sets Ω_{e_V} and $\Omega_{\tilde{\omega}_V}$ can be arbitrarily small, and the errors e_V and $\tilde{\omega}_V$ can also be arbitrarily small.

The above analysis process proves the stability of the closed-loop control system and ensures that the correct error e_V is bounded, but it cannot ensure that the velocity tracking error $\tilde{V}$ is bounded such that the control task still has the risk of failure. To illustrate that $\tilde{V}$ is bounded, further analysis is performed as follows.

Step 2 Prove that $\tilde{V}$ is bounded.

It has been proved that e_V and $\tilde{\omega}_V$ are bounded, and because $\left|\phi_V\mathrm{sgn}(\xi_V)\xi_V^2/\left(\xi_V^2 + \beta_V\right)\right| < \phi_V$ is also bounded, it is known from Eq. (27) that $\boldsymbol{\Phi}_{\mathrm{c}}$ is bounded. Combining with the Assumption 1, we can see that there must be a bounded constant $\vartheta_{\boldsymbol{\Phi}}$

$$|\boldsymbol{\Phi} - \boldsymbol{\Phi}_c| \le \vartheta_{\boldsymbol{\Phi}} \tag{77}$$

Select the following Lyapunov function

$$W_1 = \frac{1}{2}\xi_V^2 \tag{78}$$

Taking time derivative along Eq. (78) and invoking Eq. (24), we get

$$\begin{aligned}\dot{W}_1 &= \xi_V\dot{\xi}_V\\ &= -\phi_V\mathrm{sgn}^2(\xi_V)\frac{\xi_V^3}{\xi_V^2 + \beta_V} + k_V\xi_V(\boldsymbol{\Phi} - \boldsymbol{\Phi}_{\mathrm{c}})\\ &\le -\phi_V\frac{|\xi_V|^3}{\xi_V^2 + \beta_V} + k_V|\xi_V|\vartheta_{\boldsymbol{\Phi}}\\ &= -|\xi_V|\left(\phi_V\frac{|\xi_V|^2}{\xi_V^2 + \beta_V} - k_V\vartheta_{\boldsymbol{\Phi}}\right)\end{aligned} \tag{79}$$

If $\phi_V > \phi_V|\xi_V|^2/\left(\xi_V^2 + \beta_V\right) > k_V\vartheta_{\boldsymbol{\Phi}}$, then $\dot{W}_1 < 0$. So the closed-loop system is globally uniformly ultimately stable, and ξ_V is globally uniformly ultimately bounded.

Therefore, $\tilde{V} = e_V + \xi_V$ is also bounded. □

4.2 Stability analysis for altitude subsystem

Theorem 5 *For the altitude subsystem of AHV [Eq. (17)], considering the amplitude and rate*

saturation of actuator δ_e [*Eqs.* (40) *and* (41)], *and using the designed control laws* (49), (58) *and the adaptive law* (56), *then the closed-loop control system is semi-globally uniformly ultimately stable, and the path angle tracking error* $\tilde{\gamma}$ *is bounded.*

Proof Prove in three steps.

Step 1 Prove that $\tilde{\delta}_e$ is bounded.

First, it is explained that the elevator execution error $\tilde{\delta}_e$ is bounded. From Eq. (67), there is a bounded constant ς_M such that

$$\left|\dot{\hat{\delta}}_{ec} - \dot{\delta}_{ec}\right| \le \varsigma_M \tag{80}$$

Substituting Eq. (63) into Eq. (62), we obtain

$$\begin{aligned} \dot{e}_\delta &= \omega_{ec} - \dot{\delta}_{ec} + \phi_\delta \mathrm{sgn}(\xi_\delta)\frac{\xi_\delta^2}{\xi_\delta^2+\beta_\delta} \\ &= -k_{\delta 1}e_\delta - k_{\delta 2}\int_0^t e_\delta \mathrm{d}\tau + \dot{\hat{\delta}}_{ec} - \dot{\delta}_{ec} \end{aligned} \tag{81}$$

Take the following Lyapunov function

$$W_\delta = \frac{e_\delta^2}{2} + \frac{k_{\delta 2}}{2}\left(\int_0^t e_\delta \mathrm{d}\tau\right)^2 \tag{82}$$

Take time derivative along Eq. (82) and invoke Eq. (81)

$$\begin{aligned} \dot{W}_\delta &= e_\delta \dot{e}_\delta + k_{\delta 2}e_\delta \int_0^t e_\delta \mathrm{d}\tau \\ &= e_\delta\left[-k_{\delta 1}e_\delta - k_{\delta 2}\int_0^t e_\delta d\tau + \dot{\hat{\delta}}_{ec} - \dot{\delta}_{ec}\right] \\ &\quad + k_{\delta 2}e_\delta \int_0^t e_\delta \mathrm{d}\tau \\ &= -k_{\delta 1}e_\delta^2 + e_\delta\left(\dot{\hat{\delta}}_{ec} - \dot{\delta}_{ec}\right) \end{aligned} \tag{83}$$

Combining with Eq. (80), we can see

$$\begin{aligned} \dot{W}_\delta &\le -k_{\delta 1}e_\delta^2 + e_\delta \varsigma_M \\ &\le -\left(k_{\delta 1} - \frac{1}{2}\right)e_\delta^2 + \frac{1}{2}\varsigma_M^2 \end{aligned} \tag{84}$$

Let $k_{\delta 1} > 1/2$ and define the following compact sets

$$\Omega_\delta = \left\{ e_\delta \middle| |e_\delta| \le \sqrt{\varsigma_M^2/(2k_{\delta 1}-1)} \right\} \tag{85}$$

If $e_\delta \notin \Omega_\delta$, then $\dot{W}_\delta < 0$. Therefore, the closed-loop control system is semi-globally uniformly ultimately stable, and the error e_δ is semi-globally uniformly ultimately bounded, and eventually converges into the compact set Ω_δ.

$\left|\phi_\delta \mathrm{sgn}(\xi_\delta)\xi_\delta^2/\left(\xi_\delta^2+\beta_\delta\right)\right| < \phi_\delta$ is bounded, so ω_{ec} is bounded by Eq. (63). Combining Eq. (41), it can be derived that ω_e is bounded, so there must be a bounded constant ϑ_δ so that

$$|\omega_e - \omega_{ec}| \le \vartheta_\delta \tag{86}$$

Select the following Lyapunov function

$$W_2 = \frac{1}{2}\xi_\delta^2 \tag{87}$$

Take time derivative along Eq. (87) and invoke Eq. (60)

$$\begin{aligned} \dot{W}_2 &= \xi_\delta \dot{\xi}_\delta \\ &= -\phi_\delta \mathrm{sgn}^2(\xi_\delta)\frac{\xi_\delta^3}{\xi_\delta^2+\beta_\delta} + \xi_\delta(\omega - \omega_{ec}) \\ &\le -\phi_\delta \frac{|\xi_\delta|^3}{\xi_\delta^2+\beta_\delta} + |\xi_\delta|\vartheta_\delta \\ &= -|\xi_\delta|\left(\phi_\delta \frac{|\xi_\delta|^2}{\xi_\delta^2+\beta_\delta} - \vartheta_\delta\right) \end{aligned} \tag{88}$$

If $\phi_\delta > \phi_\delta|\xi_\delta|^2/(\xi_\delta^2+\beta_\delta) > \vartheta_\Phi$, then $\dot{W}_2 < 0$, so ξ_δ is globally uniformly ultimately bounded.

Therefore, $\tilde{\delta}_e = e_\delta + \xi_\delta$ is bounded. The following shows that e_γ is also bounded.

Step 2 Prove that e_γ is bounded.

Replacing the ideal control law δ_{ec} in Eq. (48) with the correct control law δ_{ec}^*, we get

$$\begin{aligned} \dot{\hat{E}}' &= F_h(x,\delta_e) + k_h\delta_{ec}^* - \dddot{\hat{\gamma}}_d + \frac{\phi_{h1}\mathrm{sgn}(\xi_{h3})\xi_{h1}^2}{\xi_{h1}^2+\beta_{h1}} \\ &\quad + \phi_{h2}\frac{\xi_{h2}^2}{\xi_{h2}^2+\beta_{h2}} + \frac{\phi_{h3}\mathrm{sgn}(\xi_{h3})\xi_{h3}^2}{\xi_{h3}^2+\beta_{h3}} + 3\lambda\ddot{\hat{e}}_\gamma \\ &\quad + 3\lambda^2\dot{\hat{e}}_\gamma + \lambda^3 e_\gamma \end{aligned} \tag{89}$$

Taking into account the elevator deflection rate constraint problem, the following two cases are analyzed.

Case 1 The elevator deflection rate is not constrained and the control law δ_e can be effectively performed. At this point, $\delta_{ec}^* = \delta_{ec}$ is known from Eq. (58). In combination with Eqs. (49), (55) and (56), then Eq. (89) can be changed to

$$\dot{\hat{E}}' = -k_{h1}\hat{E}' - \frac{1}{2}\hat{E}'\hat{\omega}_h \boldsymbol{h}^{\mathrm{T}}(\boldsymbol{X}_2)\boldsymbol{h}(\boldsymbol{X}_2) + \boldsymbol{W}_h^{*\mathrm{T}} h(\boldsymbol{X}_2) + \iota \tag{90}$$

Define estimation error of ω_h

$$\tilde{\omega}_h = \hat{\omega}_h - \omega_h \tag{91}$$

Select the following Lyapunov function

$$W_h = \frac{1}{2}\hat{E}'^2 + \frac{\tilde{\omega}_h^2}{2\mu_h} \tag{92}$$

Taking time derivative along Eq. (92) and invoking Eqs. (57), (90) and (91), we obtain

$$\begin{aligned}\dot{W}_h &= \hat{E}'\dot{\hat{E}}' + \frac{\tilde{\omega}_h\dot{\hat{\omega}}_h}{\mu_h} \\ &= \hat{E}'\left[-k_{h1}\hat{E}' - \frac{1}{2}\hat{E}'\hat{\omega}_h\boldsymbol{h}^{\mathrm{T}}(\boldsymbol{X}_2)\boldsymbol{h}(\boldsymbol{X}_2) + W_h^{*\mathrm{T}}\boldsymbol{h}(\boldsymbol{X}_2) + \iota\right] + \frac{\tilde{\omega}_h}{\mu_h}\left[\frac{\mu_h}{2}\hat{E}'^2\boldsymbol{h}^{\mathrm{T}}(\boldsymbol{X}_2)\boldsymbol{h}(\boldsymbol{X}_2) - 2\hat{\omega}_h\right] \\ &= -k_{h1}\hat{E}'^2 - \frac{1}{2}\hat{E}'^2\omega_h\boldsymbol{h}^{\mathrm{T}}(\boldsymbol{X}_2)\boldsymbol{h}(\boldsymbol{X}_2) + \hat{E}'W_h^{*\mathrm{T}}\boldsymbol{h}(\boldsymbol{X}_2) + \hat{E}'\iota - \frac{2\tilde{\omega}_h\hat{\omega}_h}{\mu_h}\end{aligned} \tag{93}$$

Since,

$$\hat{E}'\boldsymbol{W}_h^{*\mathrm{T}}\boldsymbol{h}(\boldsymbol{X}_2) \le \frac{\hat{E}'^2}{2}\left\|\boldsymbol{W}_h^{*\mathrm{T}}\boldsymbol{h}(\boldsymbol{X}_2)\right\|^2 + \frac{1}{2}$$

$$\frac{2\tilde{\omega}_h\hat{\omega}_h}{\mu_h} \ge \frac{\tilde{\omega}_h^2}{\mu_h} - \frac{\omega_h^2}{\mu_h}$$

$$\hat{E}'\iota \le \left|\hat{E}'\iota\right| \le \frac{\hat{E}'^2}{4} + \iota_{\mathrm{M}}^2$$

According to the Cauchy–Schwarz inequality

$$\left\|\boldsymbol{W}_h^{*\mathrm{T}}\boldsymbol{h}(\boldsymbol{X}_2)\right\| \le \left\|\boldsymbol{W}_h^*\right\|\left\|\boldsymbol{h}(\boldsymbol{X}_2)\right\|$$

Further,

$$\begin{aligned}\hat{E}'\boldsymbol{W}_h^{*\mathrm{T}}\boldsymbol{h}(\boldsymbol{X}_2) &\le \frac{\hat{E}'^2}{2}\left\|\boldsymbol{W}_h^*\right\|^2\left\|\boldsymbol{h}(\boldsymbol{X}_2)\right\|^2 + \frac{1}{2} \\ &= \frac{\hat{E}'^2}{2}\omega_h\boldsymbol{h}^{\mathrm{T}}(\boldsymbol{X}_2)\boldsymbol{h}(\boldsymbol{X}_2) + \frac{1}{2}\end{aligned}$$

Then, Eq. (93) can be transformed to

$$\dot{W}_h \le -\left(k_{h1} - \frac{1}{4}\right)\hat{E}'^2 - \frac{\tilde{\omega}_h^2}{\mu_h} + \frac{1}{2} + \iota_{\mathrm{M}}^2 + \frac{\omega_h^2}{\mu_h} \tag{94}$$

Let $k_{h1} > 1/4$ and define the following compact sets

$$\begin{aligned}\Omega_{\hat{E}'} &= \left\{\hat{E}'\left|\left|\hat{E}'\right| \le \sqrt{\left(\frac{1}{2} + \iota_{\mathrm{M}}^2 + \frac{\omega_h^2}{\mu_h}\right)\Big/\left(k_{h1} - \frac{1}{4}\right)}\right.\right\} \\ \Omega_{\tilde{\omega}_h} &= \left\{\tilde{\omega}_h\left|\left|\tilde{\omega}_h\right| \le \sqrt{\left(\frac{1}{2} + \iota_{\mathrm{M}}^2 + \frac{\omega_h^2}{\mu_h}\right)\Big/\left(\frac{1}{\mu_h}\right)}\right.\right\}\end{aligned} \tag{95}$$

If $\hat{E}' \notin \Omega_{\hat{E}'}$ or $\tilde{\omega}_h \notin \Omega_{\tilde{\omega}_h}$, then $\dot{W}_h < 0$. Therefore, $\hat{E}'$ and $\tilde{\omega}_h$ are semi-globally uniformly ultimately bounded and eventually can be converged to $\Omega_{\hat{E}'}$ and $\Omega_{\tilde{\omega}_h}$, respectively. By choosing appropriate parameters, $\Omega_{\hat{E}'}$ and $\Omega_{\tilde{\omega}_h}$ can be arbitrarily small, and the errors $\hat{E}'$ and $\tilde{\omega}_h$ can also be arbitrarily small.

Case 2 The elevator deflection rate is constrained and the control law δ_{e} cannot be effectively executed. At this point, we can see from Eqs. (58) and (59) that

$$\delta_{\mathrm{ec}}^* = \delta'_{\mathrm{ec}} = \delta_{\mathrm{ec}} + \tilde{\delta}_{\mathrm{e}} \tag{96}$$

In combination with Eqs. (49), (55), (56) and (96), Eq. (89) can be transformed to

$$\dot{\hat{E}}' = -k_{h1}\hat{E}' - \frac{1}{2}\hat{E}'\hat{\omega}_h\boldsymbol{h}^{\mathrm{T}}(\boldsymbol{X}_2)\boldsymbol{h}(\boldsymbol{X}_2) + \boldsymbol{W}_h^{*\mathrm{T}}\boldsymbol{h}(\boldsymbol{X}_2) + \iota + k_h\tilde{\delta}_{\mathrm{e}} \tag{97}$$

It has been proved that $\tilde{\delta}_{\mathrm{e}}$ is bounded, so there must be a nonnegative bounded constant κ_M such that

$$\left|\tilde{\delta}_{\mathrm{e}}\right| \le \kappa_M \tag{98}$$

The analysis process is the same as that in case 1, and combined with Eqs. (98), (94) can become

$$\dot{W}_h \le -\left(k_{h1} - \frac{1}{4}\right)\hat{E}'^2 - \frac{\tilde{\omega}_h^2}{\mu_h} + \frac{1}{2} + \iota_{\mathrm{M}}^2 + \frac{\omega_h^2}{\mu_h} + k_h\kappa_M \tag{99}$$

Also let $k_{h1} > 1/4$ and change the compact set (95) to

$$\begin{aligned}\Omega'_{\hat{E}'} &= \left\{\hat{E}'\left|\left|\hat{E}'\right| \le \sqrt{\left(\frac{1}{2} + \iota_{\mathrm{M}}^2 + \frac{\omega_h^2}{\mu_h} + k_h\kappa_M\right)\Big/\left(k_{h1} - \frac{1}{4}\right)}\right.\right\} \\ \Omega'_{\tilde{\omega}_h} &= \left\{\tilde{\omega}_h\left|\left|\tilde{\omega}_h\right| \le \sqrt{\left(\frac{1}{2} + \iota_{\mathrm{M}}^2 + \frac{\omega_h^2}{\mu_h} + k_h\kappa_M\right)\Big/\left(\frac{1}{\mu_h}\right)}\right.\right\}\end{aligned}$$

If $\hat{E}' \notin \Omega'_{\hat{E}'}$ or $\tilde{\omega}_h \notin \Omega'_{\tilde{\omega}_h}$, then $\dot{W}_h < 0$. Therefore, at this time, $\hat{E}'$ and $\tilde{\omega}_h$ are also semi-globally uniformly ultimately bounded, and eventually converge to $\Omega'_{\hat{E}'}$ and $\Omega'_{\tilde{\omega}_h}$, respectively.

From the analysis of cases 1 and 2, it can be seen that $\hat{E}'$ and $\tilde{\omega}_h$ are always bounded regardless of whether the elevator deflection rate is constrained. The following further illustrates that E' is bounded.

Define estimation error of FD

$$\begin{cases} v_1 = \hat{z}_2 - z_2, v_2 = \hat{z}_3 - z_3 \\ v_3 = \dot{\hat{\gamma}}_\mathrm{d} - \dot{\gamma}_\mathrm{d}, v_4 = \ddot{\hat{\gamma}}_\mathrm{d} - \ddot{\gamma}_\mathrm{d}, v_5 = \dddot{\hat{\gamma}}_\mathrm{d} - \dddot{\gamma}_\mathrm{d} \end{cases} \tag{100}$$

According to Eq. (67), there is $v_{iM} \in \mathbf{R}^+$ such that

$$v_i \le v_{iM} (i = 1, 2, \ldots, 5) \tag{101}$$

Combine Eqs. (43) (47) and (100)

$$\begin{aligned} E' &= \hat{E}' + (z_3 - \hat{z}_3 + \ddot{\hat{\gamma}}_\mathrm{d} - \ddot{\gamma}_\mathrm{d}) \\ &\quad + 3\lambda(z_2 - \hat{z}_2 + \dot{\hat{\gamma}}_\mathrm{d} - \dot{\gamma}_\mathrm{d}) \\ &= \hat{E}' + v_4 - v_2 + 3\lambda(v_3 - v_1) \end{aligned} \tag{102}$$

Considering Eq. (100), then Eq. (102) becomes

$$E' \le \hat{E}' + v_{4M} + v_{2M} + 3\lambda(v_{3M} + v_{1M}) \tag{103}$$

Therefore, E' is bounded and further e_γ is also bounded. The following further proves the boundedness of $\tilde{\gamma}$.

Step 3 Prove that $\tilde{\gamma}$ is bounded.

For polynomial $-3\lambda\ddot{\hat{e}}_\gamma - 3\lambda^2\dot{\hat{e}}_\gamma - \lambda^3 e_\gamma$ in $\delta_{\mathrm{ec}0}$ [Eq. (49)], according to Eq. (44), (46) and (100), we have

$$\begin{aligned} &-3\lambda\ddot{\hat{e}}_\gamma - 3\lambda^2\dot{\hat{e}}_\gamma - \lambda^3 e_\gamma \\ &\quad = -3\lambda\left(\ddot{e}_\gamma + v_2 - v_4\right) \\ &\qquad - 3\lambda^2\left(\dot{e}_\gamma + v_1 - v_3\right) - \lambda^3 e_\gamma \\ &\qquad \le -3\lambda\ddot{e}_\gamma - 3\lambda^2\dot{e}_\gamma - \lambda^3 e_\gamma \\ &\qquad + 3\lambda(v_{2\mathrm{M}} + v_{4\mathrm{M}}) + 3\lambda^2(v_{1\mathrm{M}} + v_{3\mathrm{M}}) \end{aligned} \tag{104}$$

And $\left|\phi_{hi}\xi_{hi}^2/\left(\xi_{hi}^2 + \beta_{hi}\right)\right| < \phi_{hi} (i = 1, 2, 3)$ is bounded. Since $\hat{E}'$, $\tilde{\omega}_h$, and e_γ have been proved to be bounded, it can be known that δ_{ec} is bounded by combining Remark 4 and Eq. (56). Therefore, there must be a nonnegative bounded constant $\vartheta_{\delta_\mathrm{e}}$ such that $|\delta_\mathrm{e} - \delta_{\mathrm{ec}}| \le \vartheta_{\delta_\mathrm{e}}$.

Select the following positive Lyapunov function

$$\begin{aligned} W_3 &= \phi_{h2}\int_0^{\xi_{h1}} \frac{\tau_1^2}{\left|\tau_1^2\right| + \beta_{h1}} \mathrm{d}\tau_1 \\ &\quad + \phi_{h2}\int_{\xi_{h1}}^{\xi_{h2}} \frac{\tau_2^2}{\left|\tau_2^2\right| + \beta_{h2}} \mathrm{d}\tau_2 + \frac{\xi_{h3}^2}{2} \end{aligned} \tag{105}$$

Taking time derivative along Eq. (105) and invoking Eq. (42), we get

$$\begin{aligned} \dot{W}_3 &= \phi_{h2}\frac{\xi_{h1}^2}{\xi_{h1}^2 + \beta_{h1}}\dot{\xi}_{h1} + \left(\phi_{h2}\frac{\xi_{h2}^2}{\xi_{h2}^2 + \beta_{h2}}\dot{\xi}_{h2}\right. \\ &\quad \left. - \phi_{h2}\frac{\xi_{h1}^2}{\xi_{h1}^2 + \beta_{h1}}\dot{\xi}_{h1}\right) + \xi_{h3}\dot{\xi}_{h3} \\ &= \xi_{h3}\mathrm{sgn}(\xi_{h3})\left[-\phi_{h1}\frac{\xi_{h1}^2}{\xi_{h1}^2 + \beta_{h1}} - \phi_{h3}\frac{\xi_{h3}^2}{\xi_{h3}^2 + \beta_{h3}}\right. \\ &\quad \left. + k_h(\delta_\mathrm{e} - \delta_{\mathrm{ec}})\right] \\ &\le -\left[\phi_{h1}\frac{\xi_{h1}^2}{\xi_{h1}^2 + \beta_{h1}} + \phi_{h3}\frac{\xi_{h3}^2}{\xi_{h3}^2 + \beta_{h3}} - k_h\vartheta_{\delta_\mathrm{e}}\right]|\xi_{h3}| \end{aligned} \tag{106}$$

If $\phi_{h1} > \phi_{h1}\xi_{h1}^2/(\xi_{h1}^2 + \beta_{h1}) > k_h\vartheta_{\delta_\mathrm{e}}$ or $\phi_{h3} > \phi_{h3}\xi_{h3}^2/(\xi_{h3}^2 + \beta_{h3}) > k_h\vartheta_{\delta_\mathrm{e}}$, then $\dot{W}_3 < 0$. Therefore, the system (42) is uniformly stable, and its state variables ξ_{h1}, ξ_{h2} and ξ_{h3} are bounded. So it can be further seen that $\tilde{\gamma} = e_\gamma + \xi_{h1}$ is also bounded. □

5 Simulation results

With AHV longitudinal motion model [Eqs. (1)–(7)] as the controlled object, the tracking simulation of velocity and altitude reference commands is performed using a fourth-order Runge–Kutta method. The simulation step length is set to 0.01 s and the simulation period is set to 300 s. The initial state value of AHV is shown in Table 1. The velocity reference command V_ref and the altitude reference command h_ref are given by the following second-order system

$$\frac{V_\mathrm{ref}(s)}{V_I(s)} = \frac{h_\mathrm{ref}(s)}{h_I(s)} = \frac{\omega_n^2}{s^2 + 2\zeta_n\omega_n s + \omega_n^2} \tag{107}$$

where damping ratio $\zeta_n = 0.9$; natural frequency $\omega_n = 0.1$ rad/s; V_I is a step signal with a step amplitude of 150 m/s per 100 s; h_I is a square wave signal with an amplitude of 200 m and a period of 200 s.

To verify the robustness of the control law, suppose that there is the following perturbation of 40% in AHV model

$$D = \begin{cases} D_0, & 50i \le t < 50(i+1) \\ D_0[1 + 0.4\sin(0.1\pi t)], & 50(i+1) \le t < 50(i+2) \end{cases}$$

where $i = 0, 2, 4$; D_0 represents nominal value; D stands for simulation value.

At the same time, the external disturbance d_1 is added in Eq. (1), and the external disturbance d_2 is added in Eq. (5). Their expressions are as follows

$$\begin{cases} d_1 = d_2 = 0, & 0\text{s} \le t < 150\text{s} \\ d_1 = 2\sin(0.1\pi t), d_2 = 0.02\sin(0.1\pi t), & t > 150\text{s} \end{cases}$$

The simulation uses control laws (27), (58) and adaptive laws (38), (57). The control law design parameters are selected as: $k_V = 0.9$, $k_{V1} = 0.3$, $k_{V2} = 0.8$, $k_{\gamma 1} = 2$, $k_{\gamma 2} = 0.1$, $k_h = 0.9$, $k_{h1} = 50$, $k_{\delta 1} = k_{\delta 2} = 1$ and $\lambda = 7$; the adaptive design parameters are: $\mu_V = \mu_h = 0.05$; auxiliary system design parameters are taken as: $\phi_V = 1$, $\beta_V = \beta_{h1} = \beta_{h2} = \beta_{h3} = 0.1$, $\phi_{h1} = 0.5$, $\phi_{h2} = \phi_{h3} = 1$, $\phi_\delta = 0.1$ and $\beta_\delta = 0.5$; FD design parameters are taken as:$R_1 = R_2 = 0.05$, $R_3 = 2$, $a_{11} = a_{13} = a_{21} = a_{23} = 0.5$, $a_{12} = a_{14} = a_{22} = a_{24} = 0.1$, $a_{31} = 2$, $a_{32} = 1$; the numbers of RBFNN nodes are taken as $N_1 = N_2 = 20$; in the velocity subsystem, the center $\boldsymbol{c}_1$ of the Gaussian function is evenly spaced within [2500 m/s, 3100 m/s] × [− 0.1, 1], and its width $\boldsymbol{b}_1$ is taken as 6.56; in altitude subsystem, the center $\boldsymbol{c}_2$ of

Table 1 Initial trim conditions

Item	Value	Unit
V	2500	m/s
h	27,000	m
γ	0	○
θ	1.5295	○
Q	0	○/s
η_1	0.2857	–
η_2	0.2350	–

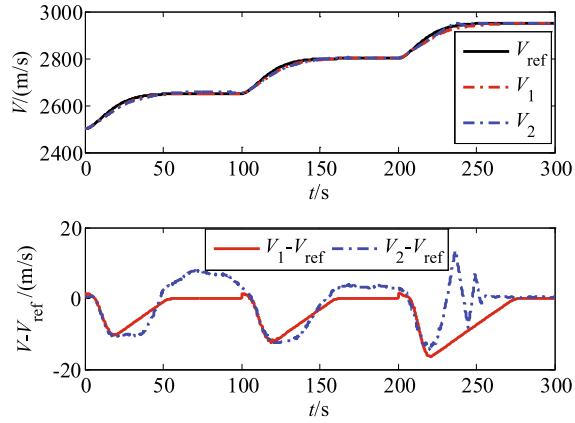

Fig. 3 Velocity tracking performance of Example 1

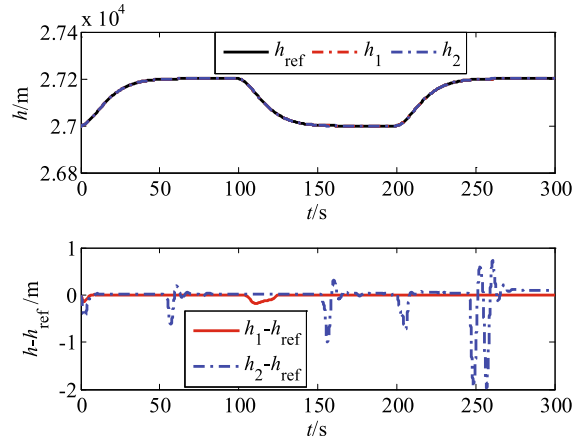

Fig. 4 Altitude tracking performance of Example 1

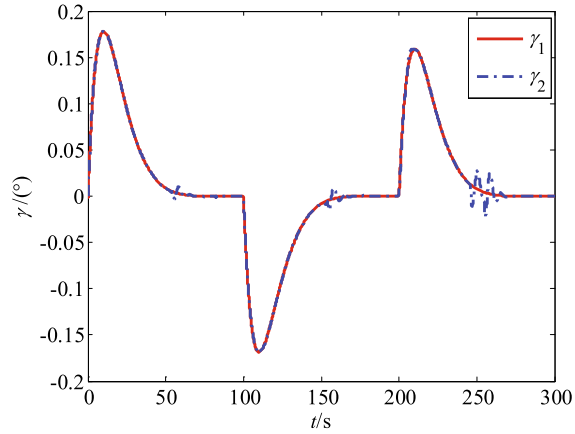

Fig. 5 Flight-path angle of Example 1

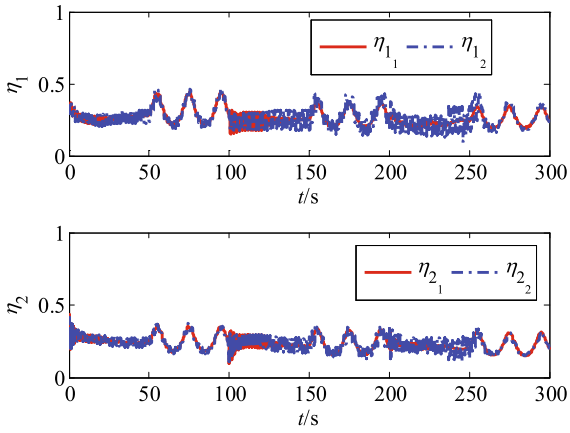

Fig. 6 Flexible states of Example 1

Gaussian function is evenly spaced in $[-1^\circ, 1^\circ] \times [0^\circ, 5^\circ] \times [-5^\circ/s\ , 5^\circ/s\ ] \times [0\ \text{rad}, 0.35\ \text{rad}]$; the width $\boldsymbol{b}_2$ is selected as 0.01. The simulation is carried out in the following three examples.

Example 1 Under the above simulation conditions, considering that the control inputs amplitude are constrained, their executable range is taken as $\Phi \in [0.05, 1]$ and $\delta_e \in [-18^\circ, 18^\circ]$. In the simulation figures, the subscript "1" represents the result of adopting the method of this paper, and the subscript "2" represents the result of adopting the method in Ref. [43] (Figs. 3, 4, 5, 6, 7, 8, 9).

Example 2 Further consider that the control input rate is also constrained, set the actuator control constraints to $\Phi \in [0.05, 1]$, $\delta_e \in [-18^\circ, 18^\circ]$ and $\dot{\delta}_e \in [-50^\circ/\text{s}\ , 50^\circ/\text{s}\ ]$. Use the method in Ref. [43] for simulation (Figs. 10, 11, 12, 13, 14, 15).

Example 3 Considering that the actuator amplitude and rate are both constrained, the actuator constraints are the same as those in case 2, which is taken as $\Phi \in [0.05, 1]$, $\delta_e \in [-18^\circ, 18^\circ]$ and

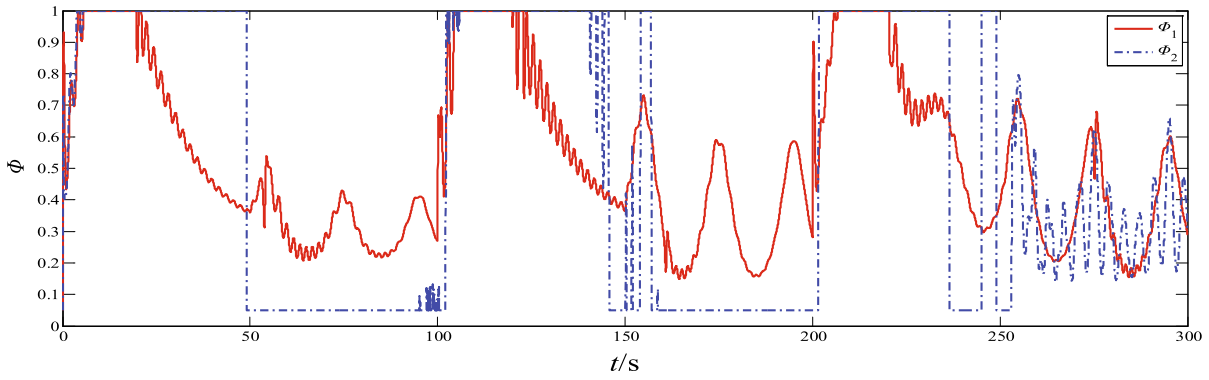

Fig. 7 Fuel-air equivalence ratio of Example 1

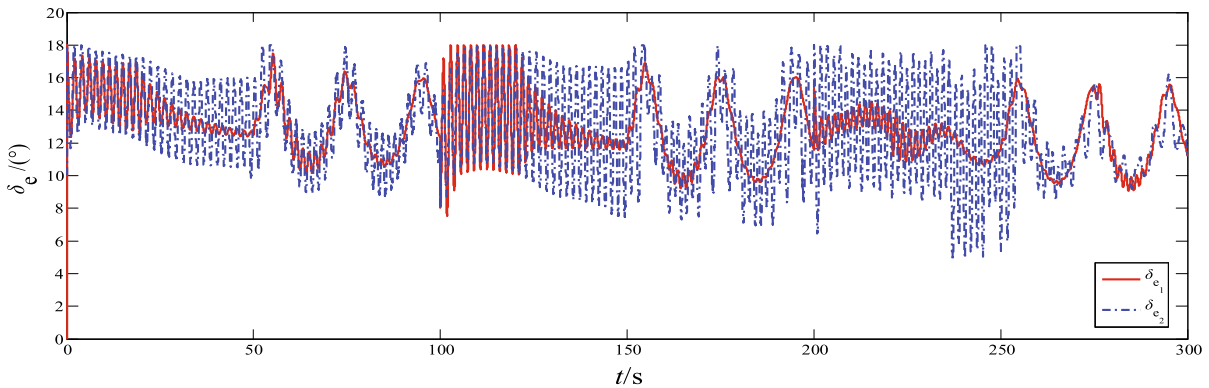

Fig. 8 Elevator angular deflection of Example 1

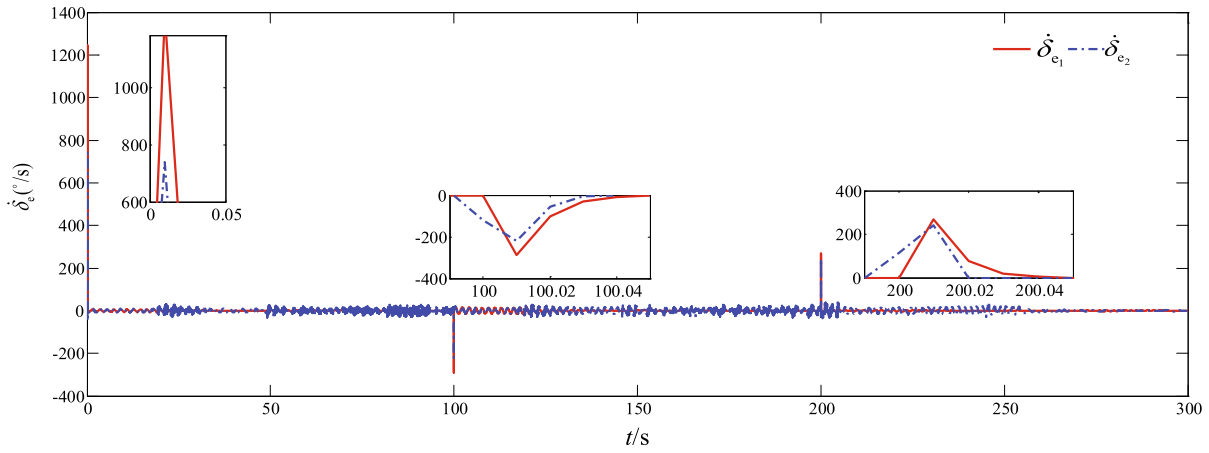

Fig. 9 Rate of elevator angular deflection of Example 1

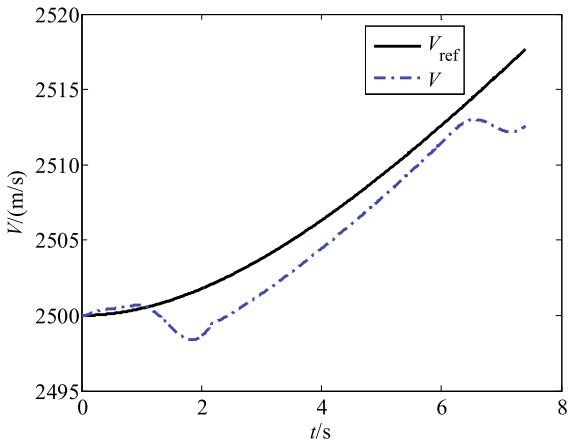

Fig. 10 Velocity tracking performance of Example 2

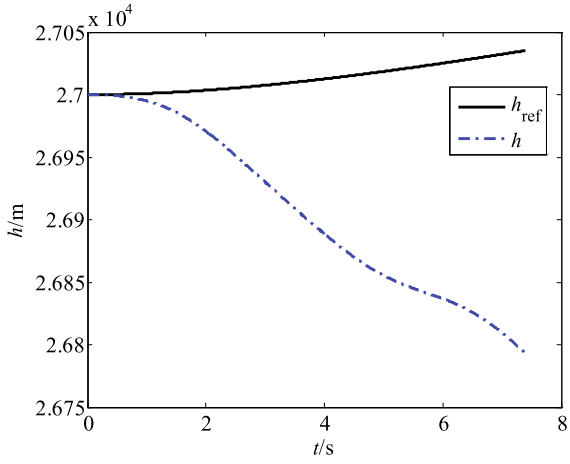

Fig. 11 Altitude tracking performance of Example 2

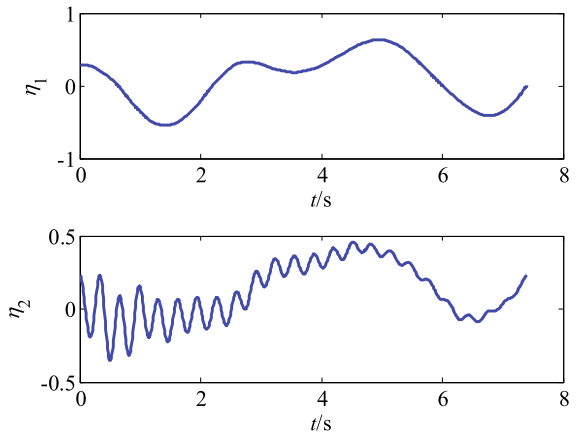

Fig. 12 Flexible states of Example 2

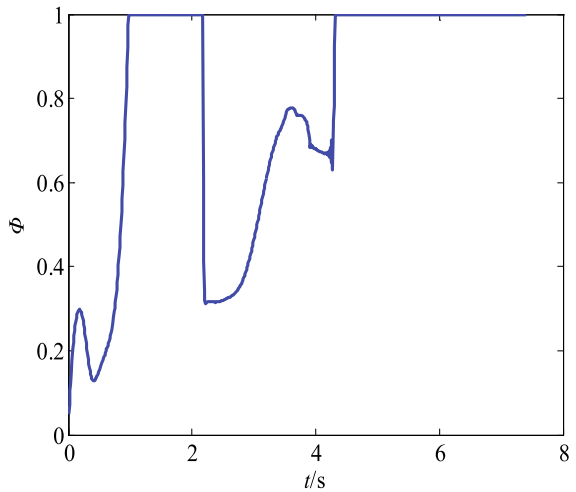

Fig. 13 Fuel-air equivalence ratio of Example 2

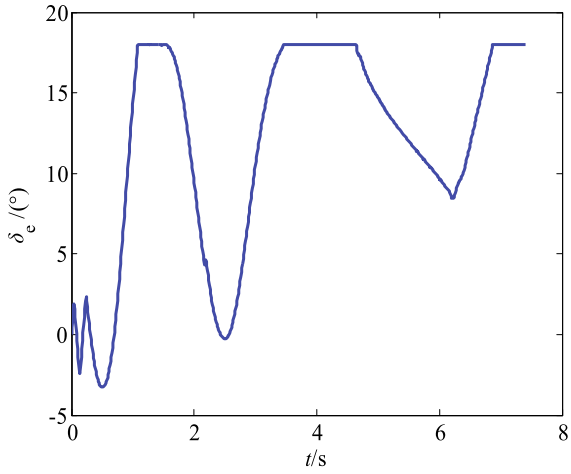

Fig. 14 Elevator angular deflection of Example 2

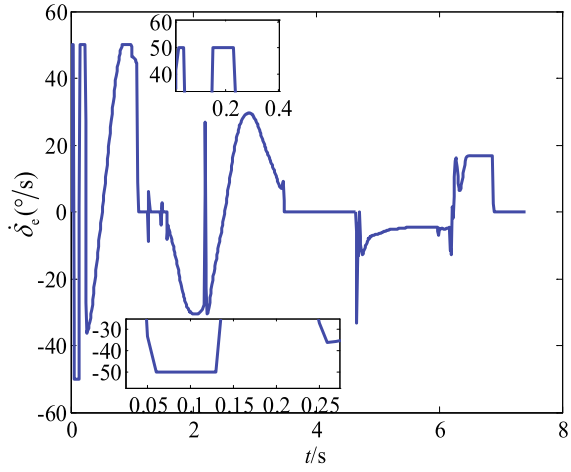

Fig. 15 Rate of elevator angular deflection of Example 2

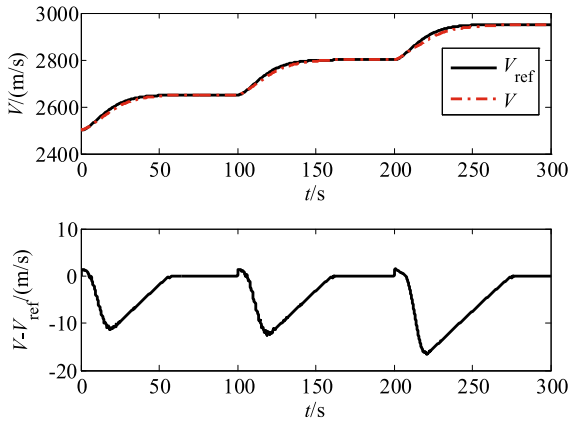

Fig. 16 Velocity tracking performance of Example 3

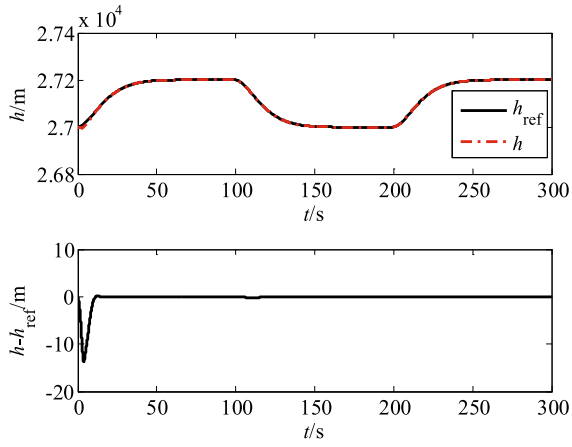

Fig. 17 Altitude tracking performance of Example 3

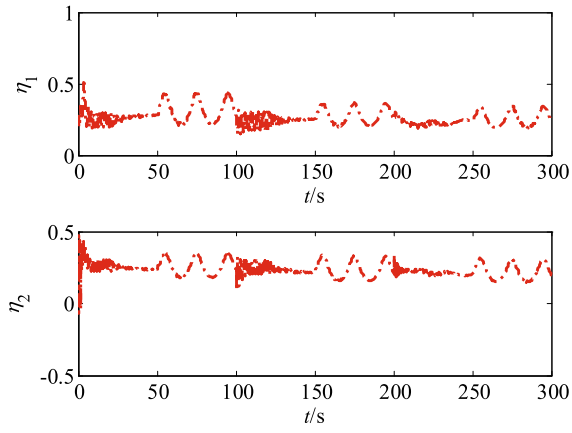

Fig. 18 Flexible states of Example 3

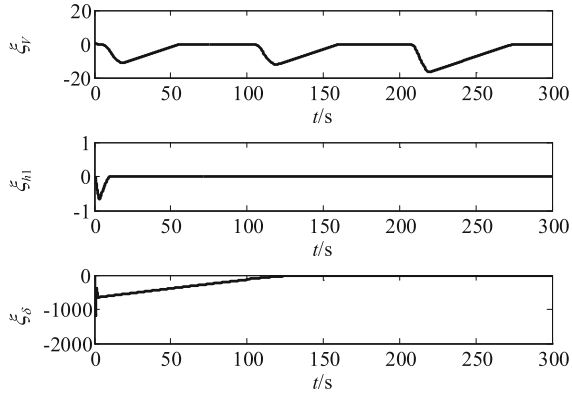

Fig. 19 Auxiliary error compensation of Example 3

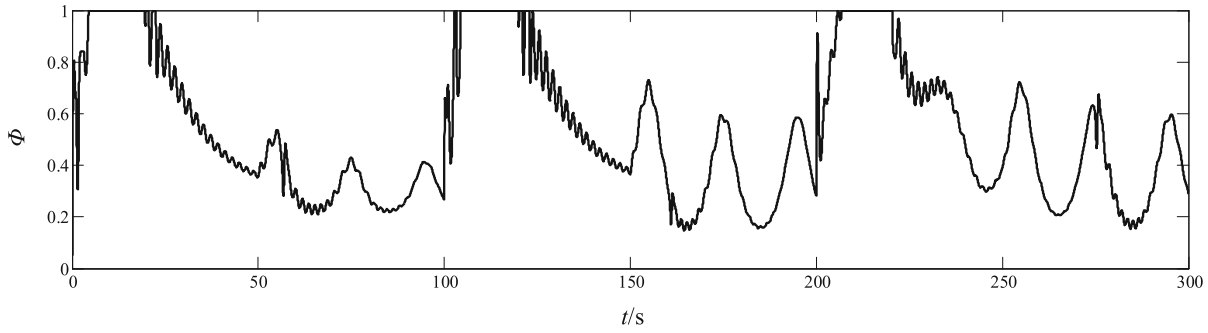

Fig. 20 Fuel-air equivalence ratio of Example 3

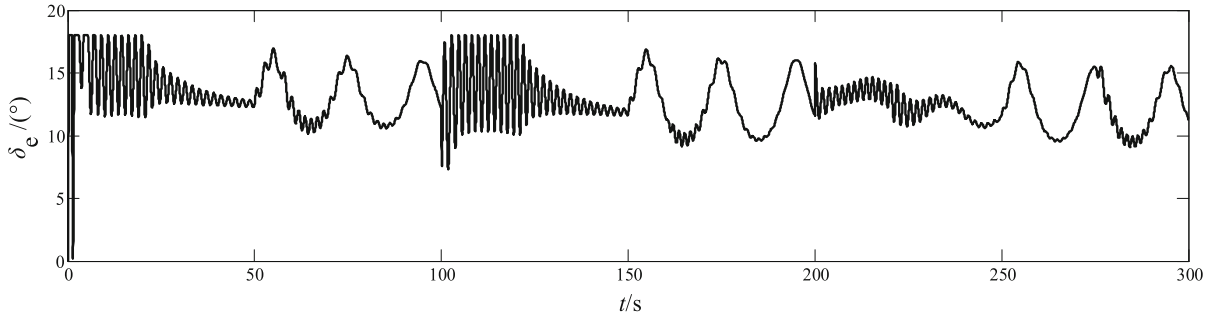

Fig. 21 Elevator angular deflection of Example 3

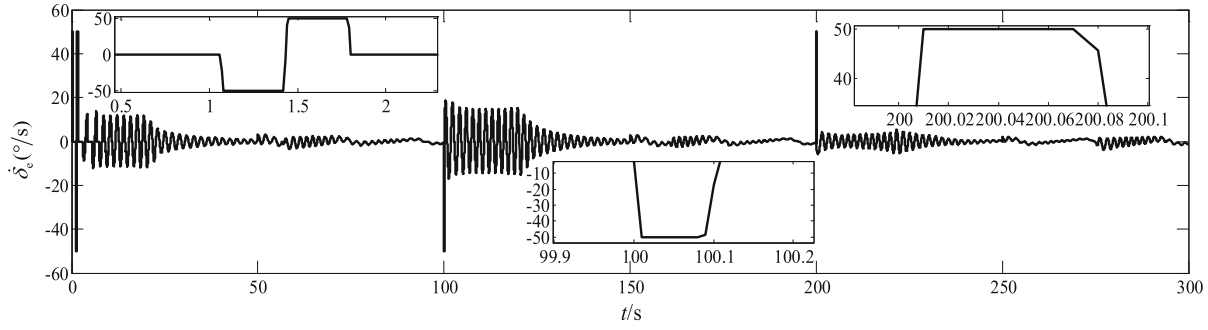

Fig. 22 Rate of elevator angular deflection of Example 3

$\dot{\delta}_e \in [-50^\circ/s, 50^\circ/s]$. Use the method proposed in this paper to simulate (Figs. 16, 17, 18, 19, 20, 21, 22).

From the above simulation results, we can see that when the amplitude of the actuator of the AHV is constrained but the rate is not (see Figs. 7, 8 and 9), the method proposed in this paper or the method in Ref. [43] can guarantee V and h stably track the respective reference commands (see Figs. 3 and 4) . And both of them can effectively suppress the flexible vibration of the AHV (see Fig. 6). However, the tracking accuracy and anti-interference ability of the proposed method are slightly better than those in Ref. [43] (see Figs. 3 and 4). Further, when both the amplitude and rate of the actuator of the AHV are constrained (see Figs. 13, 14 and 15), the stability of the closed-loop control system cannot be guaranteed by the method in Ref. [43] (see Figs. 10 and 11). But using the method designed in this paper, even if Φ, δ_e, and $\dot{\delta}_e$ are all constrained (see Fig. 20, 21 and 22), V and h can still stably track the reference commands (see Figs. 16 and 17) by the effective compensation of

the auxiliary system (see Fig. 19). And it can effectively suppress the flexible vibration (see Fig. 18).

Remark 6 On one hand, in [43], forcibly simplifying non-affine motion model of AHV to affine motion model will inevitably result in the loss of some key kinematic characteristics. However, in this paper, the control law designed for the AHV non-affine motion model is more reliable. In addition, different from Ref. [43], the high-order differential signal is accurately estimated by using FD in this paper, which reduces the influence of external noise on the control system and further improves the anti-interference ability and robustness of the control system.

On the other hand, in [43], by adopting relevant methods to modify the ideal control law, only the condition of actuator amplitude constraint can be dealt with, but its rate constraint is not compensated in any way. Therefore, when the amplitude and rate of the actuator are constrained at the same time, if the control method in [43] is used, the control system may diverge. In contrast, in this paper, by designing a new type of auxiliary system to repeatedly modify the ideal control law, the stability of the closed-loop control system can be guaranteed when the amplitude and rate of the actuator are simultaneously constrained.

6 Conclusion

(1) For the flexible AHV model, when the actuator amplitude is constrained and the control inputs are saturated, the control method designed in this paper can effectively compensate for the saturation state, thus ensuring the stability of the closed-loop control system.
(2) When there are parametric perturbation and external strong interference in the AHV model, the control method designed in this paper reflects strong robustness and anti-interference capability.
(3) When further considering a situation closer to reality that both amplitude and rate of actuator are constrained, different from existing studies, the method designed in this paper can still achieve the velocity and altitude stably tracking their respective reference commands.

In addition, this paper and most of the existing papers often only focus on its saturation characteristics when considering the constraint of AHV's actuators. However, the actual AHV's actuator has more complicated nonlinear characteristics. Therefore, in view of the complex nonlinear characteristics of the AHV's actuator, further research on the AHV's input constraint control method will be the next step.

Acknowledgements The authors would like to express their sincere thanks to the editor and anonymous reviewers for their helpful suggestions for improving the technical note.

Funding This work was supported by the National Natural Science Foundation of China (Grant nos. 61873278 and 61773398).

Compliance with ethical standards

Conflict of interest The authors declare that they have no conflict of interest.

References

1. Bertin, J.J., Cummings, R.M.: Fifty years of hypersonics: where weve been, where were going. Prog. Aerosp. Sci. **39**, 511–536 (2003)
2. Morelli, E.A.: Flight-test experiment design for characterizing stability and control of hypersonic vehicles. J. Guid. Control Dyn. **32**(3), 949–959 (2009)
3. Preller, D., Smart, M.K.: Longitudinal control strategy for hypersonic accelerating vehicles. J. Spacecr. Rockets **52**(3), 993–998 (2015)
4. Duan, H.B., Li, P.: Progress in control approaches for hypersonic vehicle. Sci. China Technol. Sci. **55**(10), 2965–2970 (2012)
5. Xu, B., Shi, Z.K.: An overview on flight dynamics and control approaches for hypersonic vehicles. Sci. China Inf. Sci. **58**, 1–18 (2015)
6. Sun, C.Y., Mu, C.X., Yu, Y.: Some control problems for near space hypersonic vehicles. Acta Autom. Sin. **39**(11), 1901–1913 (2013)
7. Gang, G., Jinzhi, W.: Reference command tracking control for an air-breathing hypersonic vehicle with parametric uncertainties. J. Frankl. Inst. **350**, 1155–1188 (2018)
8. Zhang, L.X., Nie, L., Cai, B., Yuan, S., Wang, D.Z.: Switched linear parameter-varying modeling and tracking control for flexible hypersonic vehicle. Aerosp. Sci. Technol. **95**, 105445 (2019)
9. Hu, C.F., Wei, X.F., Ren, Y.L.: Passive fault-tolerant control based on weighted LPV Tube-MPC for air-breathing hypersonic vehicles. Int. J. Control Autom. Syst **17**, 1–14 (2019)
10. Wang, Z.H., Shi, P., Lim, C.C.: H_-/H_∞ fault detection observer in finite frequency domain for linear parameter-varying descriptor systems. Automatica **86**, 38–45 (2017)

11. Xu, Y., Dong, J.G., Lu, R.Q., Xie, L.H.: Stability of continuous-time positive switched linear systems: a weak common copositive Lyapunov functions approach. Automatica **97**, 278–285 (2018)
12. Zhao, Y., Cai, G.B., Zhang, S.X.: Design of LPV anti-windup model reference control system for hypersonic vehicles. Electron. Opt. Control **26**(1), 61–67 (2019)
13. Zhao, Y., Cai, G.B., Zhang, S.X., Hou, M.Z.: Design offinite-time LPV sliding mode controller for hypersonic vehicle. J. Harbin Inst. Technol. **51**(4), 107–114 (2019)
14. Hu, C.F., Yang, N., Ren, Y.L.: Polytopic linear parameter varying model-based tube model predictive control for hypersonic vehicles. Int. J. Adv. Robot. Syst. **14**(3), 1–13 (2017). https://doi.org/10.1177/1729881417714398
15. Wei, X., Liu, L., Wang, Y.J.: Reliability-based linear parameter varying robust non-fragile control for hypersonic vehicles with disturbance observer. Clust. Comput. J. Netw. Softw. Tools Appl. **22**, 6709–6728 (2019)
16. Guanghui, W., Xiuyun, M.: Nonlinear disturbance observer based robust backstepping control for a flexible air-breathing hypersonic vehicle. Aerosp. Sci. Technol. **54**, 174–182 (2016)
17. Wang, X., Guo, J.: Robust nonsingular Terminal sliding mode backstepping control for air-breathing hypersonic vehicles. Acta Aeronaut. Astronaut. Sin. **38**(3), 320287 (2017)
18. Tang, X.N., Zhai, D., Li, X.J.: Adaptive fault-tolerance control based finite-time backstepping for hypersonic flight vehicle with full state constrains. Inf. Sci. **507**, 53–66 (2020)
19. Dong, C.Y., Liu, Y., Wang, Q.: Barrier Lyapunov function based adaptive finite-time control for hypersonic flight vehicles with state constraints. ISA Trans. **96**, 163–176 (2020)
20. Zhu, Y.Z., Zheng, W.X.: Multiple Lyapunov functions analysis approach for discrete-time switched piecewise-affine systems under dwell-time constraints. Autom. Control, IEEE Trans (2019). https://doi.org/10.1109/TAC.2019.2938302
21. Zhang, S., Wang, Q., Yang, G., Zhang, M.J.: Anti-disturbance backstepping control for air-breathing hypersonic vehicles based on extended state observer. ISA Trans. **92**, 84–93 (2019)
22. Wang, F., Guo, Y., Wang, K., Zhang, Z., Hua, C.C., Zong, Q.: Disturbance observer based robust backstepping control design of flexible air-breathing hypersonic vehicle. IET Control Theory Appl. **13**(4), 572–583 (2019)
23. Tan, S.L., Lei, H.M., Wang, P.F.: Backstepping control for hypersonic vehicle with a novel tracking differentiator. J. Astronaut. **40**(6), 673–683 (2019)
24. Wang, X., Guo, J., Tang, S.J., Qi, S.: Fixed-time disturbance observer based fixed-time back-stepping control for an air-breathing hypersonic vehicle. ISA Trans. **88**, 233–245 (2019)
25. Liu, L., Liu, Y.J., Tong, S.C.: Neural networks-based adaptive finite-time fault-tolerant control for a class of strict-feedback switched nonlinear systems. IEEE Trans. Cybern. **49**(7), 2536–2545 (2019)
26. Wang, H., Liu, P.X., Bao, J., Xie, X.-J., Li, S.: Adaptive neural output-feedback decentralized control for large-scale nonlinear systems with stochastic disturbances. Neural Netw. Learn. Syst, IEEE Trans (2019). https://doi.org/10.1109/TNNLS.2019.2912082
27. Wang, H.Q., Liu, S.W., Yang, X.B.: Adaptive neural control for non-strict-feedback nonlinear systems with input delay. Sci. Inf. (2019). https://doi.org/10.1016/j.ins.2019.09.043
28. Huo, X., Ma, L., Zhao, X.D., Niu, B., Zong, G.D.: Observer-based adaptive fuzzy tracking control of MIMO switched nonlinear systems preceded by unknown backlash-like hysteresis. Inf. Sci. **490**, 369–386 (2019)
29. Bu, X.W., Wu, X.Y., Ma, Z., et al.: Novel adaptive neural control of flexible air-breathing hypersonic vehicles based on sliding mode differentiator. Chin. J. Aeronaut. **28**(4), 1209–1216 (2015)
30. Xia, R.S., Chen, M., Wu, Q.X., Wang, Y.H.: Neural network based integral sliding mode optimal flight control of near space hypersonic vehicle. Neurocomputing. **379**, 41–52 (2020)
31. Zhang, X.F., Chen, K., Fu, W.X., Huang, H.Q.: Neural network-based stochastic adaptive attitude control for generic hypersonic vehicles with full state constraints. Neurocomputing **351**, 228–239 (2019)
32. Zhao, H.W., Liang, Y.: Prescribed performance dynamic neural network control for a flexible hypersonic vehicle with unknown control directions. Adv. Mech. Eng. (2019). https://doi.org/10.1177/1687814019841489
33. Luo, H., Yin, S., Liu, T.Y., Khan, A.Q.: A data-driven realization of the control-performance-oriented process monitoring system. IEEE Trans. Ind. Electron. **67**(1), 521–530 (2020)
34. Cheng, X.L., Wang, P., Tang, G.J.: Fuzzy-reconstruction-based robust tracking control of an air-breathing hypersonic vehicle. Aerosp. Sci. Technol. **86**, 694–703 (2019)
35. Wang, Y.Y., Yang, X.X., Yan, H.C.: Reliable fuzzy tracking control of near-space hypersonic vehicle using aperiodic measurement information. IEEE Trans. Ind. Electron. **66**(12), 9439–9447 (2019)
36. Liu, H.D., Bao, W.M., Li, H.F., Liao, Y.X.: Multivariable disturbance observer-based fuzzy fast terminal sliding mode attitude control for a hypersonic vehicle. J. Aerosp. Eng. (2019). https://doi.org/10.1061/(ASCE)AS.1943-5525.0000991
37. Li, J., Zuo, B.: Adaptive terminal sliding mode control for air-breathing hypersonic vehicles under control input constraints. Acta Aeronaut. Astronaut. Sin. **33**(2), 220–233 (2012)
38. Xu, B., Shi, Z.K., Yang, C.G., et al.: Neural control of hypersonic flight vehicle model via time-scale decomposition with throttle setting constraint. Nonlinear Dyn. **73**, 1849–1861 (2013)
39. Bing, H., Aijun, L., Bin, X.: Adaptive fault tolerant control for hypersonic vehicle with external disturbance. Int. J. Adv. Robot. Syst. **14**(1), 1–7 (2017). https://doi.org/10.1177/1729881416687136
40. Qinglei, H., Yao, M.: Adaptive backstepping control for air-breathing hypersonic vehicle with actuator dynamics. Aerosp. Sci. Technol. **67**, 412–421 (2017)
41. Guangfu, M., Chen, C.: Adaptive backstepping-based neural network control for hypersonic reentry vehicle with input constraints. IEEE Access **6**, 1954–1966 (2018)
42. Zhonghua, W., Jingchao, L.: Tracking error constrained robust adaptive neural prescribed performance control for

flexible hypersonic flight vehicle. Int. J. Adv. Robot. Syst. **14**(1), 1–16 (2017). https://doi.org/10.1177/1729881416682704
43. Xiangwei, B., Xiaoyan, W.: Neural-approximation-based robust adaptive control of flexible air-breathing hypersonic vehicles with parametric uncertainties and control input constraints. Inf. Sci. **346**, 29–43 (2016)
44. Bolender, M.A., Doman, D.B.: Nonlinear longitudinal dynamical model of an air-breathing hy-personic vehicle. J. Spacecr. Rockets **44**(2), 374–387 (2007)
45. Parker, J.T., Serrani, A., Yurkovich, S., et al.: Control-oriented modeling of an air-breathing hypersonic vehicle. J. Guid. Control Dyn. **30**(3), 856–869 (2007)
46. Fiorentini, L., Serrani, A.: Adaptive restricted trajectory tracking for a non-minimum phase hypersonic vehicle model. Automatica **48**, 1248–1261 (2012)
47. Xu, B., Su, F., Liu, H., et al.: Adaptive Kriging controller design for hypersonic flight vehicle via back-stepping. IET Control Theory Appl. **6**(4), 487–497 (2012)
48. Luo, C.X., Lei, H.M., Zhang, D.Y., Zou, X.J.: Adaptive Neural control of hypersonic vehicles with actuator constraints. J. Aerosp. Eng. Int. (2018). https://doi.org/10.1155/2018/1284753
49. Bu, X.W., Lei, H.M.: A fuzzy wavelet neural network-based approach to hypersonic flight vehicle direct nonaffine hybrid control. Nonlinear Dyn. **94**(3), 1657–1668 (2018)
50. Sanner, R., Slotine, J.: Gaussian networks for direct adaptive control. IEEE Trans. Neural Netw. **3**(6), 837–863 (1992)
51. Park, J.H., Huh, S.H., Kim, S.H., et al.: Direct adaptive controller for nonaffine nonlinear systems using self-structuring neural networks. IEEE Trans. Neural Netw. **16**(2), 414–422 (2005)
52. Calise, A.J., Hovakimyan, N., Idan, M.: Adaptive output feedback control of nonlinear systems using neural networks. Automatica **37**(1), 1201–1211 (2001)
53. Wang, X.H., Chen, Z.Q., Yang, G.: Finite-time-convergent differentiator based on singular perturbation technique. IEEE Trans. Autom. Control **52**(9), 1731–1737 (2007)